Linköping Studies in Science and Technology. Licentiate Thesis No. 1900

High-Temperature Fatigue in a Steam Turbine Steel

Modelling of Cyclic Deformation and Crack Closure

Ahmed Azeez

Linköping Studies in Science and Technology
Licentiate Thesis No. 1900

High-Temperature Fatigue in a Steam Turbine Steel

Modelling of Cyclic Deformation and Crack Closure

Ahmed Azeez

Division of Solid Mechanics
Department of Management and Engineering
Linköping University
SE–581 83 Linköping, Sweden

Linköping, March 2021

Cover:
Scanning electron microscope image of a fracture surface from a smooth cylindrical specimen of the steam turbine steel FB2 tested under fully reversed low cycle fatigue at 600 °C and 0.8 % total strain range. The visible striations (linear marks) indicate fatigue crack growth.

Printed by:
LiU-Tryck, Linköping, Sweden, 2021
ISBN: 978-91-7929-696-4
ISSN: 0280-7971

Distributed by:
Linköping University
Department of Management and Engineering
SE–581 83 Linköping, Sweden

This document was prepared with LaTeX, February 16, 2021

Preface

The research I present in this licentiate thesis is part of my ongoing PhD investigation and summarises my work conducted at the Division of Solid Mechanics, Linköping University, over the period 2018–2020. This thesis has been divided into two main parts. Part II, "Appended Papers", present my specific research work in the form of published/to-be-published scientific articles. Part I of the thesis, "Background and Summary", provide an overview of my research topics and summarises my work. Part I also provides general background knowledge with motivation to my work and how it fits within the literature, while Part II represents my primary research focus.

Special gratitude goes to my supervisor, Robert Eriksson. His mentoring and guidance is undeniable. I'm glad I still have more years to work with you. Many thanks to my co-supervisors and all involved in my project, Kjell Simonsson, Daniel Leidermark, Mattias Calmunger, Viktor Norman, Johan Moverare, Henning Almstedt, and Torsten-Ulf Kern. Looking forward to more research and more fruitful discussions. I thank all my colleagues at Linköping University for all the good times and the many more to come.

Special thanks to my family, my parents and my siblings, for their never-ending care and support. To my friend and wife, Ulkar, no words can describe my gratitude to you, an incredible companion and support.

Ahmed Azeez
احمد عثمان عزيز

Linköping, February 2021

Abstract

Existing conventional thermal power plants are retrofitted for flexible operations to assist the transition toward more renewable energies. The deployment of many renewable energy power plants is necessary to achieve a clean environment with less pollution. However, the intermittent nature of renewable energies, due to weather changes, and the lack of efficient large energy storage systems put renewables at a disadvantage. Flexible operations of power plants imply fast and frequent start-ups. Thus, retrofitted power production plants can be utilised as an energy backup to satisfy the immediate demand during peak energy times or when renewable energies are suddenly limited.

Large thermal power plants generally employ steam turbines with high inlet temperature and pressure steam conditions. Materials used for components at the high-temperature turbine sections are expected to withstand harsh environments. The use of 9–12 % Cr martensitic steels is desirable due to, among other things, their superior resistance to creep for temperatures up to 625 °C. Retrofitting for flexible operations put steam turbine components under high-temperature fatigue loading conditions different from how they were designed before. The flexible operations could lead to fatigue cracking at critical locations, such as grooves and notches at the inner steam turbine casing. Thus, fatigue behaviour understanding of steam turbine materials under such loading conditions is essential for components life prediction. Accurate and less conservative fatigue life prediction approach is necessary to extend the turbine components life, which reduces waste and provides economic benefits. This can be done by extending operations past crack initiation phase and allowing controlled propagation of cracks in the components.

Within the 9–12 % Cr steel class, the martensitic steam turbine steel called FB2 is studied under high-temperature fatigue. This includes investigating high-temperature fatigue life behaviour, cyclic deformation behaviour, stress relaxation behaviour, and crack propagation behaviour along with crack closure behaviour. This was achieved by experimentally testing samples made from FB2 steel under isothermal low cycle fatigue, isothermal fatigue crack propagation, and thermomechanical fatigue crack propagation.

List of papers

In this licentiate thesis, the following papers have been appended:

I. A. Azeez, R. Eriksson, D. Leidermark, M. Calmunger (2020). Low cycle fatigue life modelling using finite element strain range partitioning for a steam turbine rotor steel, *Theoretical and Applied Fracture Mechanics*, Volume 107, June 2020, Article 102510. `https://doi.org/10.1016/j.tafmec.2020.102510`

II. A. Azeez, V. Norman, R. Eriksson, D. Leidermark, J. Moverare (2020). Out-of-phase thermomechanical fatigue crack propagation in a steam turbine steel — modelling of crack closure, *International Journal of Fatigue*, Conditionally accepted.

Note
All appended papers are published/to-be-published in open access. Any reformatting of the appended papers was solely intended to fit the layout of the thesis.

Author contributions
The writing and the research in all the appended papers were carried out primarily by me. All the modelling work and the evaluation of data from testing presented in **Paper I** and **Paper II** were done by me. All the experimental testing were performed at Linköping University by Viktor Norman (TMF crack propagation tests in **Paper II**), Mattias Calmunger (Isothermal LCF tests in **Paper I**), and Johan Moverare (Isothermal crack propagation test in **Paper II**). Robert Eriksson and I did the fracture surface evaluations and the sample preparation in **Paper I**. Mattias Calmunger carried out the microstructural evaluations, EBSD maps and quantification of LAGB, in **Paper I**.

Acknowledgement

The research presented in this licentiate thesis has been produced at the Division of Solid Mechanics at Linköping University and is part of the project TURBO-REFLEX. The research has received funding from the European Union's Horizon 2020 research and innovation programme under grant agreement No. 764545, the support of which is greatly acknowledged. Siemens AG is acknowledged for their continuous support and for providing the material used in the experimental testing.

Contents

Part I

Background and Summary

1 Introduction

Steam turbines have long been used to supply energy to society in the form of electricity. Thermal power plants employing steam turbines have been relying on conventional energy sources for many years. However, renewable energy sources are becoming the world's means to proceed toward a better environment with less pollution. The intermittent nature of renewable energies and the lack of efficient large energy storage systems have put renewable energy power plants at a considerable disadvantage. Thus, to support and facilitate renewable energy power plants' deployment, integration with existing thermal power plants is needed. The integration requires the operational shift of thermal power plants from base-load operation with few start-ups and shut-downs to a flexible operation with quick and many start-ups and shut-downs. This flexible operation allows existing thermal power plants to provide energy stability and fulfil energy demand during peak times. Thus, facilitating the transition toward more renewable energies and a better environment. However, this put steam turbines under different loading conditions than what they were designed for, which might considerably limit the turbine components' life.

Under flexible operation, fatigue damage at high temperature is the limiting factor of components' life. In such harsh conditions with repeated loading, defects such as cracks start to initiate and propagate. Understanding both crack initiation and propagation would give the tools required for accurate component life predictions. Thus, investigating the material behaviour under conditions close to the actual turbine component is necessary.

In this study, a steam turbine steel, FB2, used in the high-temperature turbine sections is investigated under conditions close to those found at critical locations in the inner casing of steam turbines, such as grooves and notches. The inner casing temperature can reach up to 620 °C during operation. Sample specimens of FB2 were tested in the laboratory to obtain the cyclic deformation behaviour, stress relaxation behaviour, fatigue life behaviour, crack growth behaviour, and crack closure behaviour. Three different types of experimental testing were used: isothermal low cycle fatigue (LCF), isothermal fatigue crack propagation, and thermomechanical fatigue (TMF) crack propagation. From the LCF testing, numerical modelling of the material cyclic deformation behaviour was possible through the use of finite element (FE) method. Both elasto-plastic and creep material models were utilised to simulate the initial and the stable cyclic deformation behaviour of FB2. Microstructural investigation close to the fracture surface can be performed to investigate the fatigue damage behaviour. For FB2 steel, signs of creep damage in

the form of voids were detected at 600 °C. This suggested that creep could largely influence fatigue at elevated temperatures. Thus, the construction of fatigue life prediction models for steam turbine steels must consider the influence of creep and fatigue at high temperatures. Fatigue crack growth behaviour of steam turbine steels can be investigated using crack propagation testing. The unexpected premature opening or closing of cracks, i.e. crack closure, generally influences crack growth behaviour. Thus, understanding and predicting crack closure are necessary to account for its effects. For the steam turbine steel FB2, crack closure was detected under TMF conditions, which is close to the steam turbine inner casing conditions. A compliance-based method adapted for TMF conditions can be used to estimate the crack closure levels. For predicting crack closure levels for FB2 steel under TMF conditions, a three dimensional FE model with stationary crack and contact conditions was used.

1.1 Aims of the work

In general, this thesis work aims for a better understanding of fatigue behaviour for steam turbine steels operating at high-temperature components. This understanding is intended at facilitating the construction of accurate and less conservative life prediction approach. Thus, the work investigates the steam turbine steel FB2 under several testing conditions which are isothermal LCF, isothermal fatigue crack propagation, and TMF crack propagation.

In isothermal LCF testing, the high-temperature fatigue behaviour of FB2 is investigated. Several tests were done at different temperatures in the range of 20–625 °C including tests with dwell time to calibrate the short-term creep behaviour. Modelling temperature-dependent cyclic deformation behaviour of FB2 provided the necessary tools to explore the material behaviour using FE analysis. This allowed the construction of an appropriate life prediction model adapted for high temperatures based on strain life approach.

Components life prediction based strain life approach is limited to the initiations of cracks. However, allowing controlled growth of cracks can provide an extension to components life. Thus, fatigue crack propagation behaviour of steam turbine steels must be investigated. Fracture mechanics approach can be utilised to analyse crack growth behaviour and determine the remaining life once cracks have appeared. Both isothermal fatigue and TMF crack propagation testing of FB2 steel were performed in the current work. Crack growth behaviour under TMF conditions, i.e. close to the component conditions, provides the knowledge needed for accurate predictions. Crack closure behaviour understanding is also necessary to model accurate fatigue crack growth. Thus, predicting crack closure for FB2 steel using FE modelling provided a powerful tool to account for such behaviour.

2 Steam turbines

2.1 Background

Turbines are turbo-machineries that are generally used to produce useful mechanical work from a flowing fluid. This is typically referred to as prime mover, i.e. converting energy into work or power. Turbines can be categorised based on the type of fluid that passes through them, such as air and combustion gases in gas turbines and steam in steam turbines [1, 2].

In steam turbines, steam coming from the boiler with high temperature and high pressure is pushed through a closed casing. The turbine casing houses the rotor. The rotor consists of the main shaft with several disks. Rotating blades with an airfoil shape are generally attached to the disks. Stationary blades, which can be fixed to the casing, provide acceleration and swirl to the steam. A steam turbine stage typically contains a set of stationary blades and a set of rotating blades. During a turbine stage, the energy extraction occurs as the inlet pressurised hot steam expands through the turbine passing stationary blades and striking on the rotating blades. The torque generated by the steam forces on the rotating blades is transferred to the main shaft through the disks producing the mechanical work in the form of rotating the rotor [3, 4].

A steam turbine can have several turbine stages sharing a single rotor. This is shown for an SST5-600 steam turbine from Siemens in Fig. 1. Based on the inlet steam conditions, the turbine stages can be categorised into high-pressure, intermediate-pressure and low-pressure turbines. Different combination of these turbines, as well as more than one low-pressure turbines, can be used. This flexibility allows for an extensive range of steam turbines output capacity for different applications [1, 3, 5]. The exhaust steam from the high-pressure turbine can generally be reheated at the boiler to higher temperatures before going to the intermediate-pressure turbine. This reheating process is desirable as it increases overall efficiency.

Steam turbines are frequently used for power generation purposes, such as electricity production for industries and residents, where the rotating rotor is connected to a generator [3, 5]. However, the mechanical work from steam turbines can also be used to drive pumps or compressors to run other operations and applications [6]. Steam turbines are usually part of a large power plant that is usually classified depending on the main source of energy used to produce the steam.

Most common energy source comes from fossil fuel as in thermal power plants.

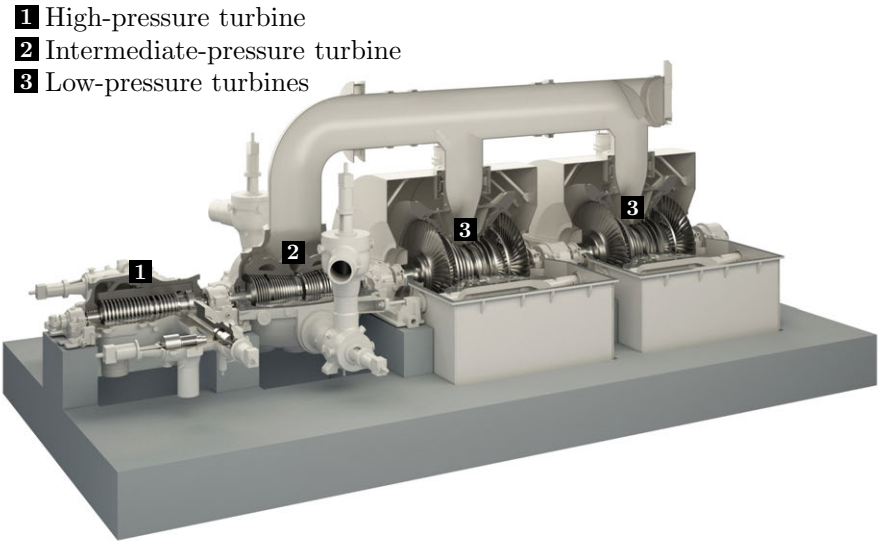

Figure 1: An SST5-6000 steam turbine set from Siemens shows high-pressure turbine, intermediate-pressure turbine and two low-pressure turbines all connected to a single rotor. Courtesy of Siemens AG.

Nevertheless, nuclear power plants and renewable energy power plants are also widely used. The use of geothermal or solar energies usually results in lower steam turbine inlet temperature and pressure [3, 7, 8]. The state of the art steam conditions for large steam turbines operating in thermal power plants have reached a main turbine inlet temperature and pressure of up to 610 °C and 300 bar, respectively, and a reheated steam temperature of up to 630 °C. These steam conditions are referred to as ultra-supercritical (USC) conditions [3, 9]. Increasing the inlet temperature and pressure would increase power production. However, steam turbines must be designed to withstand the inlet pressure and temperatures especially at the high-pressure and intermediate-pressure turbines.

2.2 Retrofitting for flexible operations

The development of renewable energies has been an essential step toward reducing emissions and environmental pollutions. Several renewable energy power plants have been built, especially for electrical power generation [10]. The transition toward clean energies must be supported by conventional energy sources such as fossil fuels, mainly due to the fluctuating nature of renewable energies and the lack of efficient and practical large energy storage systems [10]. Thus, in general, turbines are required to shift toward flexible operation to prevent energy instabilities and fulfil peak energy demands [11]. This flexibility is also demanded from turbines

operating within renewable energy power plants [12–14].

Flexible operation implies frequent and fast turbine start-ups and shut-downs. Existing steam turbines built for base-load operation must be retrofitted to achieve such flexibility. Major investigations focused on retrofitting have been followed to achieve this. The European Union funded project Turbo-Reflex (turbomachinery retrofits enabling flexible back-up capacity for the transition of the European energy system) focus on this aspect. In a broad sense, the project aims to retrofit the existing thermal power plants to enable flexible operation without penalties on components life, cost, and emissions. This is intended to back-up the energy sector and facilitate the installation of more renewable energies. The research study presented here is part of this project focusing on the mechanical integrity of steam turbines in flexible operation. Specifically, this involves investigating accurate life predictions of high-temperature components in steam turbines. In this study, a creep resistance steel is investigated under high-temperature loading conditions of the inner casing used in high-pressure and intermediate-pressure turbines operated using USC steam conditions.

The focus on turbines with USC steam conditions is motivated due to its state of the art in large thermal power plants [15]. Material deterioration under harsh conditions at high-pressure and intermediate-pressure turbines is the main limiting factor on the power plant life under flexible operation. Cracks could initiate and propagate at critical locations at the inner surface of the turbine's inner casing. Thus, it is important to examine and understand the material behaviour under flexible operation loading conditions. Determining component life help prevent unplanned events and set suitable maintenance intervals.

2.3 Loading conditions of the inner casing

The steam turbine casing is a thick-walled component that is typically produced by casting, contrary to the rotor which is typically produced through forging [16]. The casing design can be single shelled or double shelled [6]. The most common design, double shelled, includes an outer casing that supports the inner casing. The rotor is housed by the inner casing where the inlet steam passes with high pressure and temperature. The exhaust steam from the inner casing then passes to the outer casing at a lower pressure and temperature [5, 6]. In high-pressure and intermediate-pressure turbines, the inner casing wall requires large thickness due to the large pressure difference across the wall and the high steam inlet temperature, especially, in steam turbines with USC steam conditions [16].

Thick wall components, such as the inner casing, would experience large thermal stresses due to temperature gradients, especially at high-pressure and intermediate-pressure sections of the steam turbine. Flexible operation with fast loading ramps puts the inner casing under transient thermal stresses that have a major effect on the component life. Thus, it is necessary to determine the loading conditions experienced by the inner casing.

In each steam turbine cycle, i.e. start-up until shut-down, the inner casing

experiences a change in mechanical loading and temperature. The mechanical loading is caused by the temperature gradient and the steam pressure, while the temperature is determined from the steam inlet temperature. This type of loading is referred to as TMF, i.e. a variation of both mechanical loading and temperature over time. Different types of TMF cycles exist based on how the load and temperature changes over time. The inner surface of the inner turbine casing experience a cycle close to out-of-phase (OP) TMF. In OP-TMF, the maximum mechanical loading occurs at the minimum temperature and vice versa.

Figure 2 shows, schematically, the approximated OP-TMF loading condition experienced by the inner surface of the inner casing during a single steam turbine cycle. As the steam turbine starts up, the inner surface of the inner casing temperature rises, creating large temperature gradients that lead to compressive stress. This is followed by steady state condition during the turbine operation. During shut-down, the temperature drops and the stress become tensile.

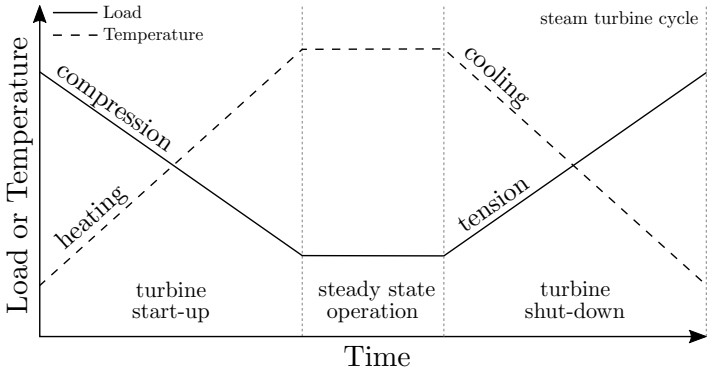

Figure 2: Thermomechanical fatigue loading conditions at the inner surface of the high temperature inner casing for a single cycle of steam turbine operation. The cycle can be mainly divided into start-up, steady state operation, and shut-down.

2.4 Steam turbine materials

The harsh conditions at high-temperature steam turbine components require the use of materials with strong mechanical and creep properties. The development of 9–12 % Cr martensitic steels has contributed to the achievement of steam turbines with USC steam inlet conditions of up to 625 °C [17–19]. These martensitic steels are favourable due to their superior resistance to long term creep [20]. The use of nickel-based alloys for steam turbines has also been of interest mainly for achieving even higher steam inlet temperatures, i.e. 700 °C [18, 21, 22]. However, as steam turbine components are generally large and thick, challenges in the manufacturing process of nickel-based alloys for such large components can be expected [22]. Besides,

nickel-based alloys are more expensive than martensitic steels. Thus, the use of nickel-based alloys could be limited to specific critical parts of the steam turbine with very high temperatures [22]. Austenitic steels have also been investigated for use as a steam turbine material that can achieve the next level of steam inlet conditions, i.e. 700 °C [23, 24]. As this thesis focuses on steam turbine steels used for USC steam condition, i.e. 9–12 % Cr martensitic steels, other steam turbine materials will not be further discussed.

A notable candidate of 9–12 % Cr martensitic steels is FB2 steel (9Cr-1Mo-1Co-0.2V-0.07Nb-0.01B-0.02N, all in wt%). The steam turbine steel FB2 was developed under the European Cooperation in Science and Technology (COST) 522 program (1998–2003) [9, 17]. This steel is commonly used for steam turbine high-temperature components due to its high resistance to creep and steam oxidation [17, 25]. As this thesis work uses FB2 steel in all its investigations [26, 27], see Part II - Appended Papers, other types of steels will not be considered in details.

The FB2 steel underwent heat treatment that is austenitisation at 1100 °C with rapid cooling followed by two tempering stages at 570 °C and 710 °C [9]. A study on FB2 by Azeez et al. [27] confirmed that the microstructure of this material was tempered martensite. FB2 steel is generally produced by forging for steam turbine rotors [19]. However, the research in this thesis, Ref. [26], uses testing based on thermomechanical loading conditions from the turbine inner casing (see Sec. 2.3), which is produced by casting [28]. This has been done to avoid the trouble of testing coarse-grained alloys.

3 Fatigue in high-temperature steels

3.1 Introduction to fatigue

Materials subjected to repeated loading could eventually fail even though the applied load did not cause immediate failure. This behaviour is attributed to a phenomenon called fatigue. Many mechanical failures in metal components are thought to be a consequence of fatigue failure [29, 30]. Designing components, that undergo cyclic loading, against fatigue is necessary to avoid unexpected failure.

Depending on the number of cycles to failure, fatigue can generally be separated into two types: high cycle fatigue (HCF) and LCF. In HCF, the applied load is usually within the elastic limit, i.e. below the material yielding point, so the fatigue life is generally long. Cycling of the material above the yield limit leads to irreversible deformation, which considerably shortens the fatigue life, as in LCF. Since the applied load is cycled, fatigue could lead to cracks in the material. In smooth surface components with no defects, the fatigue life is mostly spent in the initiation stage. Crack initiation is followed by crack growth in each cycle, which continues until a critical crack length is reached. This is when the component can no longer hold the applied load and unstable crack growth occurs, leading to rupture.

Application of cyclic stress or strain leads to mechanical fatigue. At high temperatures, time-dependent deformation due to creep plays an important role in fatigue, leading to creep-fatigue interactions. The cyclic change in temperature and mechanical loading leads to TMF, which can be observed in high-temperature turbine components.

3.2 Role of fatigue in steam turbines

In contrast to base-load operation, flexible operation demands frequent and fast start-ups of steam turbines. Flexible operation puts the turbine components under severe cyclic loading conditions where life is mainly determined by fatigue. Fast start-ups are desirable to provide quick energy output; however, high stresses can be introduced due to temperature gradients that add additional damage to the component [31]. In steam turbines with high-temperature steam conditions, both fatigue and creep play an essential role in component life since the materials used are pushed to their limits [28]. Critical components like the rotor, inner casing, main steam valve casing, and blades are commonly investigated for high-temperature fatigue damage and cracking [28, 32–36].

In thick wall components, such as high-temperature inner casings, large stresses from temperature gradients, and creep occur. Thus, critical locations, like notches and grooves, act as stress risers leading to material yielding during start-up and shut-down. This generally leads to LCF conditions where irreversible deformation occurs and cracking could happen with frequent start-ups [14, 32, 36]. Detected cracks are usually inspected to determine the possibility of their removal without compromising the component strength [32]. Undetected cracks would grow with turbine operations to critical lengths, leading to mechanical failure in an unfavourable event. However, allowing controlled growth of cracks below critical lengths can provide extended operational life for the components. Also, understanding the fatigue crack growth behaviour can prevent sudden interruption of turbines operation if cracks were to be discovered [37].

For turbines operating at USC steam conditions, i.e. high temperature and pressure inlet steam conditions, the inner casing inlet region was identified as a critical location for fatigue and creep damage [28]. The use of a single-shell casing can be beneficial for lowering costs and material usage. However, the increased temperature gradients due to lack of outer casing can introduce more stresses compared to a double-shell casing [35].

High-temperature steels used for critical steam turbine components are subjected to damage and deterioration due to fatigue and creep. Several studies on steam turbine steels have investigated high-temperature LCF and creep-fatigue interactions [27, 38–44]. The considerable creep resistance of 9-12 % Cr martensitic steels make them suitable for usage at high-temperature steam turbines components. Fatigue life predictions under TMF conditions were also investigated for 9–12 % Cr steels [45, 46]. Investigations of fatigue crack propagation behaviour for steam turbine steels have also been done [26]. The occurrence of crack closure behaviour was seen under OP-TMF conditions, i.e. close to the turbine inner casing conditions [26].

3.3 Life prediction approaches

There are different strategies to design against fatigue failure. Different stages are involved in fatigue damage. Changes at the microstructural level assist in the nucleation of permanent defects. This lead to the initiation of cracks at the microscopic level. Those tiny cracks would later grow and coincide, creating dominant cracks that would advance until instability and fracture is reached [29]. In that perspective, fatigue life, N_f, can generally be divided into the number of cycles spent on crack initiation and the number of cycles spent on crack propagation to a critical length. Both are influenced by several mechanical, microstructural, and environmental factors. Thus, different approaches to life prediction can be used depending on the dominant fatigue damage and the design philosophy. Three major life prediction approaches are commonly used: stress-life approach, strain-life approach, and fracture mechanics approach [29, 30, 47].

In smooth components with little defects, stress- and strain-life approaches

are used since the major part of life is spent under crack initiation stages. Under LCF conditions with large localised deformation, it is appropriate to characterise the fatigue life based on strains. Stress-life approach is typical for materials under HCF conditions where the stresses are not high enough to cause yielding. Stress-life approach is not further discussed in the current work. A fracture mechanics approach uses knowledge from the field of fracture mechanics to aid in the analysis of crack growth. Cracks in the components can be assumed to exist already or detected during inspections and maintenance intervals. Thus, fatigue life in fracture mechanics approach is spent propagating those cracks to critical lengths.

3.3.1 Strain-life approach

Fatigue loading that causes localised material deformation, above the material yielding point, lead to short fatigue life, i.e. LCF. Under such conditions, a strain-life approach is often used. This approach also works with lower deformations and longer fatigue life. The fatigue life estimated under this approach mostly involve the crack initiation stage. Thus, the creation of one or more macroscopic cracks that lead to noticeable damage to the component marks the end of life. Several failure criteria exist for marking the final fatigue life, N_f, as documented in testing standards [48–50]. One common failure criterion is stress-decrease, where a percentage of the drop in the maximum stress marks the final fatigue life, N_f. A drop of 25 % in the maximum stress is recommended as a failure criteria [48]. An example of stress-decrease criteria for a continuous softening material is shown in Fig. 3.

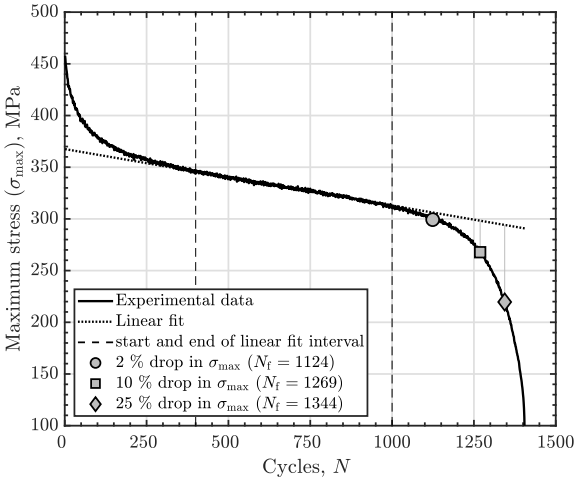

Figure 3: Stress-decrease criteria used to determine the final fatigue life, N_f, for isothermal low cycle fatigue test at 600 °C and 0.8 % total strain range of the steam turbine steel FB2 [27].

In the strain-life approach, the fatigue life is estimated base on the strain due to local yielding. The strain-life models and fatigue parameters for a material can be obtained from constant amplitude strain controlled LCF testing (see Sec. 4.1.1). As cracks usually initiate in components due to straining of localised regions, strain-controlled testing is more representative [30]. The mid-life stress-strain cycles are commonly used to extract the appropriate values of strain amplitudes used for the strain-life prediction models. Figure 4 shows an example of mid-life hysteresis loops for the steam turbine steel FB2 tested at different temperatures and applied total strain ranges, $\Delta\varepsilon_\mathrm{t}$.

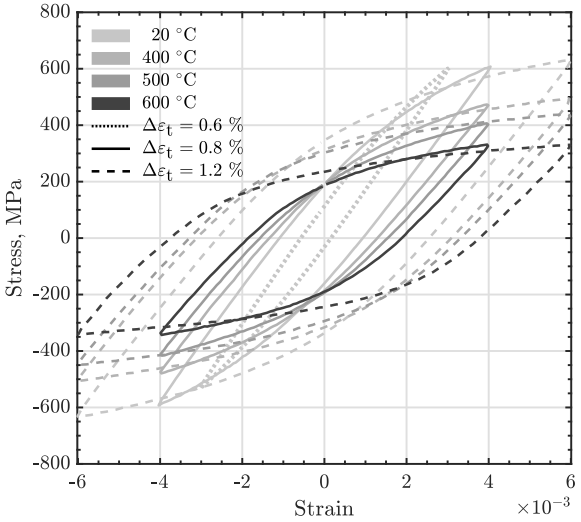

Figure 4: Mid-life hysteresis cycles of isothermal LCF tests on smooth specimens from the steam turbine steel FB2. Figure from Ref. [27].

The total strain amplitude, $\Delta\varepsilon_\mathrm{t}/2$, of the mid-life cycle can be considered as the sum of the elastic strain amplitude, $\Delta\varepsilon_\mathrm{e}/2$, and inelastic strain amplitude, $\Delta\varepsilon_\mathrm{ie}/2$, as

$$\frac{\Delta\varepsilon_\mathrm{t}}{2} = \frac{\Delta\varepsilon_\mathrm{e}}{2} + \frac{\Delta\varepsilon_\mathrm{in}}{2}, \qquad \Delta\varepsilon_\mathrm{e} = \frac{\Delta\sigma}{E}, \tag{1}$$

where $\Delta\sigma$ is the stress range and E is the elastic modulus. To characterise the fatigue life in terms of the inelastic strain amplitude, the Coffin–Manson equation is used [51]

$$\frac{\Delta\varepsilon_\mathrm{in}}{2} = \varepsilon'_\mathrm{f}\,(2N_\mathrm{f})^c \tag{2}$$

where ε'_f is the fatigue ductility coefficient and c is the fatigue ductility exponent, which are temperature dependent material constants [42]. It must be noted that

Eq. 3 is expressed in a general form using the inelastic strain amplitude, $\Delta\varepsilon_{\mathrm{ie}}/2$. The inelastic strain amplitude can be assumed as the combination of the plastic strain amplitude, $\Delta\varepsilon_{\mathrm{p}}/2$, and the creep strain amplitude, $\Delta\varepsilon_{\mathrm{c}}/2$, as

$$\frac{\Delta\varepsilon_{\mathrm{in}}}{2} = \frac{\Delta\varepsilon_{\mathrm{p}}}{2} + \frac{\Delta\varepsilon_{\mathrm{c}}}{2}. \tag{3}$$

This is followed as it was found that creep can have large influence on fatigue life at high temperatures [27]. Figure 5 shows signs of creep damage in the form of voids at the grain boundaries for the steam turbine steel FB2 tested at 600 °C under isothermal LCF conditions without dwell time [27].

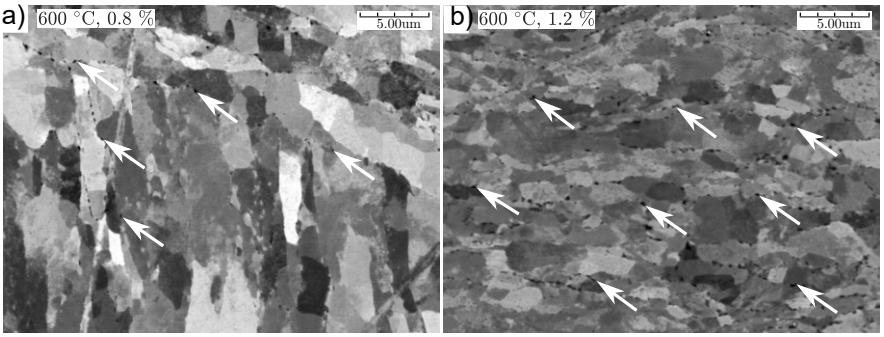

Figure 5: Backscatter electron micrographs from the specimens tested isothermally in low cycle fatigue at: (a) 600 °C, $\Delta\varepsilon_{\mathrm{t}} = 0.8$ % and (b) 600 °C, $\Delta\varepsilon_{\mathrm{t}} = 1.2$ %. The white arrows indicate visible voids at the grain boundaries. Figure from Ref. [27].

The Basquin relation can be used to relate the stress amplitude, $\Delta\sigma/2$, to the fatigue life as

$$\frac{\Delta\sigma}{2} = \sigma'_{\mathrm{f}} \left(2N_{\mathrm{f}}\right)^{b} \tag{4}$$

where σ'_{f} and b are also temperature dependent material constants [42] called the fatigue strength coefficient and exponent, respectively. The Basquin relation is suitable for longer fatigue life where the irreversible cyclic deformation is limited. Substituting Eq. 3 and Eq. 4 in Eq 5 a fatigue life model, Coffin–Manson–Basquin, in terms of total strain amplitude, $\Delta\varepsilon_{\mathrm{t}}$, can be produced

$$\frac{\Delta\varepsilon_{\mathrm{t}}}{2} = \frac{\sigma'_{\mathrm{f}}}{E} \left(2N_{\mathrm{f}}\right)^{b} + \varepsilon'_{\mathrm{f}} \left(2N_{\mathrm{f}}\right)^{c}. \tag{5}$$

This relation combine both short and long fatigue life making it useful for covering wider ranges of fatigue life.

3.3.2 Fracture mechanics approach

Fracture mechanics approach can be used to characterise fatigue crack growth. The fatigue life can be estimated as the number of fatigue cycles needed to propagate a crack with a certain length to another length or to fracture. This approach focuses on three main variables: applied stress, crack or flaw size, and fracture toughness property of the material in use [52].

Assuming linear elastic fracture mechanics (LEFM), the stress intensity factor, K, could be utilised to characterise the crack tip conditions. Three different modes of fracture exist based on how a crack is loaded, as shown in Fig. 6.

Mode I is the most common type of loading on a cracked body. Thus, the stress intensity factor discussed throughout this work will only consider Mode I. For notation simplicity, mode I stress intensity factor will just be denoted as K. The general form of K can be expressed as

$$K = \sigma_{\text{nom}} \sqrt{\pi a} f_{\text{geo}} \left(\frac{a}{W} \right) \tag{6}$$

where σ_{nom} is the applied nominal stress, a is the crack length, W is the width of the cracked body, and f_{geo} is the geometrical factor. The critical level of K at which the material can be loaded under plane strain conditions without fracture is identified as fracture toughness, K_{Ic}, a temperature-dependent material property [29]. The use of the stress intensity factor is limited to small scale yielding conditions and LEFM. Nevertheless, crack growth investigations using stress intensity factor can still be satisfactory even though some minor degree of plasticity occurred [26, 53]. Crack growth characterisation in this thesis work will only assume LEFM.

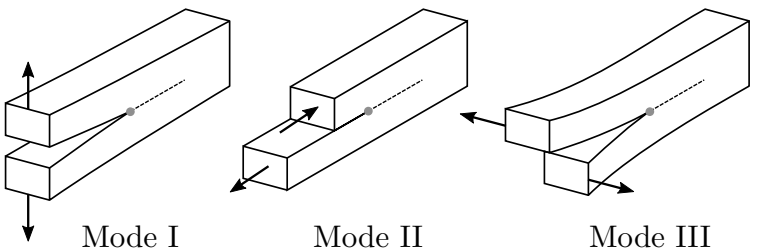

Figure 6: The three different loading modes that could be applied on a cracked body.

The critical length of a crack can be set based on the fracture toughness of the material in use. The crack propagation behaviour under constant amplitude fatigue loading can be characterised based on Paris power law relationship,

$$\frac{\mathrm{d}a}{\mathrm{d}N} = \widetilde{C} \Delta K^{\widetilde{m}} \tag{7}$$

where $\mathrm{d}a/\mathrm{d}N$ is the crack growth rate and ΔK is the stress intensity range, while $\widetilde{C}$ and $\widetilde{m}$ are material parameters. The stress intensity range, ΔK, can be defined

as

$$\Delta K = \begin{cases} K_{\max} - K_{\min} & \text{if } K_{\min} > 0 \\ K_{\max} & \text{if } K_{\min} \leq 0 \\ 0 & \text{if } K_{\max} \leq 0 \end{cases} \tag{8}$$

where $K_{\max}$ and $K_{\min}$ correspond to the stress intensity factor at the maximum and the minimum nominal stresses during a fatigue cycle, i.e. $\sigma_{\max}$ and $\sigma_{\max}$, respectively. In the definition of Eq. 8, the compressive part of the fatigue cycle is excluded, assuming the crack is fully closed under compressive stresses. Another definition includes the full stress range of the cycle producing the full stress intensity range, ΔK_{fr}, [54]

$$\Delta K_{\text{fr}} = K_{\max} - K_{\min}. \tag{9}$$

Typical fatigue crack growth behaviour for metals is schematically illustrated in Fig. 7 [52]. This log-log plot of crack growth rate versus stress intensity range shows three distinctive regions. The middle region, with intermediate values of ΔK, obey Paris power law relation presented in Eq. 7 Paris and Erdogan [55]. The other two regions deviate from linearity in the log-log plot. At low values of ΔK, the crack growth rate can decreases until no apparent crack propagation occur below. This is usually below a specific fatigue threshold value, ΔK_{th}, see Fig. 7. This threshold value is believed to depend on both the material and the load ratio [52]. At high values of ΔK, a large increase in the crack growth rate leads to unstable crack propagation and limited fatigue life. This usually happens when $K_{\max}$ approaches the fracture toughness of the material. The unstable crack growth behaviour at large ΔK values could involve considerable plasticity at the crack tip. This could invalidate LEFM and the use of the stress intensity factor. At this stage, crack growth characterisation by elastic-plastic fracture mechanics could be more appropriate [47, 52].

Besides Paris law, several other empirical relations exist in literature to describe parts or all the regions of the fatigue crack growth behaviour [29, 30, 52]. However, due to simplicity Paris law is the most used relation. It must be noted that the Paris law does not take into account mean stress effects, crack closure effects, and load ratio dependences. The increase in load ratio has been seen to increase fatigue crack growth rate, and the degree of this effect usually depends on the type of metal used. Relations developed to account for mean stress effects are mostly applicable for positive load ratios. For negative load ratios, the compression part of the cycle is usually ignored assuming that crack surfaces are closed under compression, e.g. Eq. 8. Nevertheless, the contribution from the compressive part of the fatigue cycle has been observed to affect crack growth due to crack surfaces not being completely closed, i.e. crack closure [26, 56, 57]. The steam turbine steel FB2 has been seen to experience crack closure under OP-TMF conditions, and the crack was open under compressive nominal stresses [26]. Figure 8 shows an example of several crack propagation tests performed on steam turbine steel FB2 to characterise crack growth behaviour. It can be seen that the definition of ΔK in Fig. 8 (a) and ΔK_{fr},

in Fig. 8 (b) (see Eq. 8 and 9) do not provide a unique description of the crack growth behaviour. Thus, accounting for crack closure is necessary to collapse the crack growth curves.

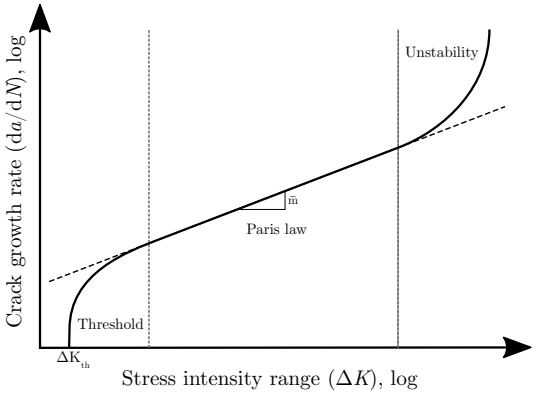

Figure 7: Illustration of fatigue crack growth behaviour for metals showing three distinctive regions. Paris law represent the linear relation in this log-log plot

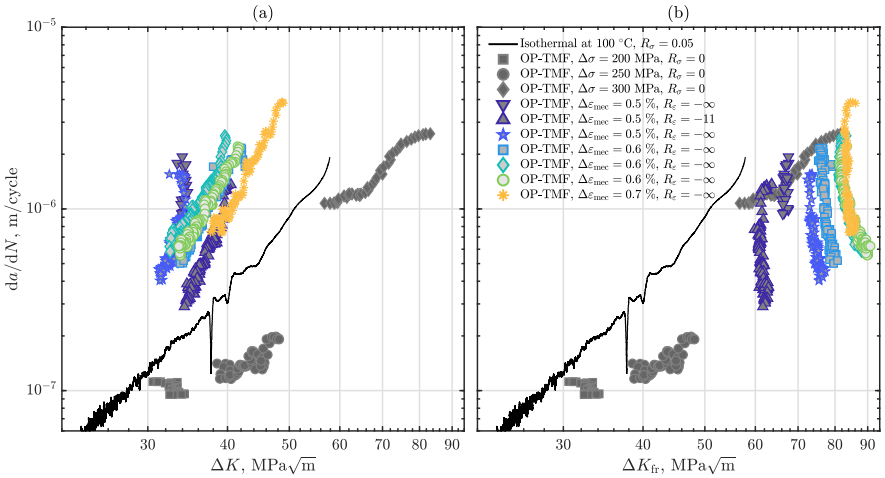

Figure 8: Fatigue crack growth behaviour of steam turbine steel FB2 without accounting for crack closure, using (a) $\mathrm{d}a/\mathrm{d}N$ versus ΔK (only tensile part of the fatigue cycles); (b) $\mathrm{d}a/\mathrm{d}N$ versus ΔK_{fr} (full range of the fatigue cycles). The crack propagation tests were performed under isothermal fatigue at 100 °C and out-of-phase thermomechanical fatigue at 100–600 °C. Figure from Ref. [26].

3.3.2.1 Crack closure

The phenomena of cracks being open under compression or being closed under tension can be referred to as crack closure behaviour. Crack closure involves unexpected closing or opening of a fatigue crack. This behaviour was discussed by Elber [58], who showed that a fatigue crack can still be open under tensile loading. Different mechanisms behind crack closure have since been identified in the literature. The most common ones are plasticity induced closure, roughness induced closure, and oxide induced closure [59, 60]. Other mechanisms, such as viscous fluid induced and transformation induced closures, were also seen [30, 52].

A change in the elastic compliance of the fatigue test specimen below or above zero nominal stress indicates crack closure behaviour. The compliance change occurs when a closed crack opens during loading and when an open crack closes during unloading. Crack closure measurement method based on changes in the compliance can be used to detect closure levels. A compliance method adapted for TMF conditions is discussed in Sec. 4.1.3.2. Figure 9 shows an example of a strain-controlled OP-TMF crack propagation test of the steam turbine steel FB2 where crack closure occurred. In Fig. 9 (a), the change in the elastic compliance of the nominal stress, σ_{nom}, versus mechanical strain, $\varepsilon_{\mathrm{mec}}$, curves indicate crack opening and crack closing below zero nominal stress, i.e. crack closure. In Fig 9 (b), the compliance method was used to determine the crack stress opening, σ_{op}, and the crack closing stress, σ_{cl}, over cycles, N. The crack opening stress represents the nominal stress at which the crack is fully open during loading, while the crack closing stress represents the nominal stress at which the crack is just starting to close during unloading. A considerable difference can be seen between σ_{op} and σ_{cl} over cycles, especially at the beginning of the test, i.e. at short crack lengths.

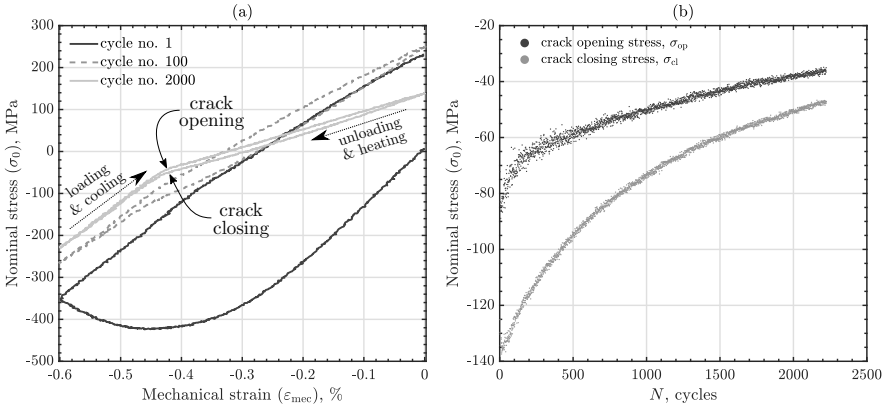

Figure 9: Out-of-phase thermomechanical fatigue crack propagation test performed at 100–600 °C with mechanical strain range of 0.6 % and strain ratio of $R_\varepsilon = -\infty$. (a) shows stress-strain curves for different cycles; (b) shows crack opening and closing stresses over cycles. Figure from Ref. [26].

The work by Elber [58] essentially described plasticity induced crack closure. This type of crack closure occurs due to the plastic zone created during cyclic loading in front of the crack tip and the wake of the deformed material on the crack faces. As plasticity induced crack closure is related to material deformation behaviour, several studies have emerged to explain crack closure using numerical modelling [60, 61]. Modelling of crack closure is discussed in Sec. 4.3. Some studies have found that residual stresses arise due to the large inelastic behaviour during the first half-cycle can be used to explain load ratio dependency and crack closure [26, 53]. To accounting for crack closure in the fatigue crack growth behaviour, the stress intensity range can be adjusted to include the part of the fatigue cycle where the crack is fully open [58]. Thus, defining the effective opening stress intensity range, $\Delta K_{\text{eff,op}}$, on the loading curve of the fatigue cycle as [26]

$$\Delta K_{\text{eff,op}} = K_{\max} - K_{\text{op}} \tag{10}$$

where K_{op} correspond to the stress intensity factor at the crack opening stress, σ_{op} (see Eq. 6). For the unloading curve of the cycle, the effective closing stress intensity range, $\Delta K_{\text{eff,cl}}$, can be defined as [26]

$$\Delta K_{\text{eff,cl}} = K_{\max} - K_{\text{cl}} \tag{11}$$

where K_{cl} is the stress intensity factor at the crack closing stress, σ_{cl} (see Eq. 6). Compensating for crack closure using an effective stress intensity range has been seen to provide appropriate correction to the fatigue crack growth data for several metals with different load ratios [26, 52, 56, 58, 62, 63]. Crack opening stress, σ_{op}, is usually used to account for the closure effects. Nevertheless, crack closing stress, σ_{cl}, has been observed to differ and normally be lower than the crack opening stress, σ_{op} [26, 64], e.g. Fig. 9 (b). A study by Azeez et al. [26] on crack closure of the steam turbine steel FB2 showed that using both effective opening and closing stress intensity ranges collapse the fatigue crack growth curves together within a small scatter band, see Fig. 10. However, the fatigue crack growth curves were seen to collapse better using the effective closing stress intensity range, $\Delta K_{\text{eff,cl}}$, see Fig. 10 (b).

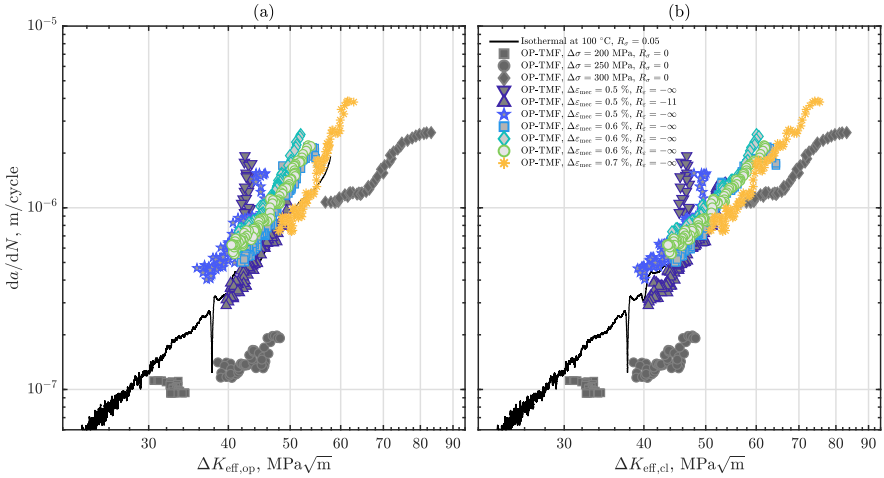

Figure 10: Fatigue crack growth behaviour of steam turbine steel FB2 accounting for crack closure, using (a) $\mathrm{d}a/\mathrm{d}N$ versus $\Delta K_{\mathrm{eff,op}}$ (closure level from the loading part of the cycle); (b) $\mathrm{d}a/\mathrm{d}N$ versus $\Delta K_{\mathrm{eff,cl}}$ (closure level from the unloading part of the cycle). The crack propagation tests were performed under isothermal fatigue at 100 °C and out-of-phase thermomechanical fatigue at 100–600 °C. Figure from Ref. [26].

3.3.3 Stretched design limits approach

A component that reaches the fatigue failure criteria set by the design approach can retire and be replaced by a new component. Even though the component has not completely failed yet, the limited knowledge of the material fatigue behaviour after the set criteria makes it dangerous for operation. Stretched design limits approach aims to combine two approaches, the strain-life and the fracture mechanics. This allows extended knowledge about fatigue behaviour even after the strain-life approach's failure criteria is reached for the component. The stretched design limits approach has also been referred to as a two-stage model [30]. Fatigue life in this approach combines the initiation of macroscopic fatigue cracks and the propagation of those cracks until critical lengths.

Extending component life provide more economic benefit as more cycles can be run safely before scraping the component. Turbine components life has been generally based on cracks initiation phase and allows little to no cracks propagation. Thus, understanding the crack growth behaviour of stream turbine steels can extend the turbine life by allowing controlled growth of cracks within safe limits. Sudden interruptions in the turbine operation can also be prevented when cracks are discovered. The fracture mechanics approach can be utilised to assess the cracks severity situation and schedules suitable maintenance interval. Hence, interruption in energy supply from turbines can be potentially reduced or avoided. The knowledge from

the stretch design limit approach can also be used to provide an optimised schedule for cracks repair. Designs such as leak-before-break can also be considered when designing turbine components under stretch design limit approach. A component replacement for steam turbines can be very costly and difficult to replace. Thus, utilising an approach that extends to include the understanding of cracks and their growth would be advantageous.

4 Experimental and numerical evaluation

4.1 Testing and methods

Exploring and understanding the behaviour of a specific material requires experimental testing and data evaluation. In testing, samples of the material are subjected to relevant loading conditions. The geometry of the samples and the loading conditions are decided based on the target application. Testing a real component under actual conditions is undesirable as it can be costly and time-consuming, as well as the produced data are too specific for general use. Thus, it is desirable to use relatively small samples to obtain the required material properties. The extracted material properties are then used to estimate the actual component behaviour through numerical or analytical models. Testing also provides the possibility of comparing the results with other materials as similar sample geometry and test set-up can be reused. Different tests exist to obtain different material properties, and specific standards exist based on previous knowledge and experience to assist with the testing.

Three different tests were used and discussed in this thesis: isothermal LCF, isothermal fatigue crack propagation, and TMF crack propagation. All the tests were carried at the material laboratory at the Division of Engineering Material, Department of Management and Engineering, Linköping University.

4.1.1 Isothermal low cycle fatigue

Isothermal LCF testing is commonly performed to obtain cyclic deformation behaviour, cyclic stress-strain curves, and fatigue resistance. Fatigue cracks in components are usually initiated in localised regions due to plastic deformation and plastic straining. Thus, strain controlled LCF testing is generally more relevant. However, strain control testing requires a more complicated test set up. Figure 11 shows the MTS servo-hydraulic test machine set up used for strain controlled isothermal LCF testing in Ref. [27]. This MTS servo-hydraulic rig is capable of running high-temperature testing using MTS 652.01 furnace. The furnace has controllable heat units, and the specimen used must be enclosed by the furnace, as shown in Fig. 11. Thermocouples attached to the specimen are used to achieve the desired testing temperature. High-temperature extensometer, Instron 2632–055, records the total mechanical strain, ε_t, of the specimen while a control unit, Instron 880, obtains the applied load, F. The extensometer is attached to the specimen at the gauge section. Generally, smooth cylindrical specimens with uniform gauge section at the

middle can be used. Figure 12 shows the detailed drawing of a button head smooth cylindrical specimen used for LCF testing in Ref. [27]. A strain-controlled LCF with fully reversed loading can be used to avoid mean stress effects. To achieve that, the strain ratio used was $R_\varepsilon = \varepsilon_{\min}/\varepsilon_{\max} = -1$; $\varepsilon_{\min}$ and $\varepsilon_{\max}$ being the minimum and maximum total mechanical strains during the cycle. During testing, applying axial load on the specimen implies uniform stress and strain within the gauge section. The nominal stress, σ_{nom}, is typically found using

$$\sigma_{\text{nom}} = \frac{F}{A_{\text{cs}}} \tag{12}$$

where F is the applied load and A_{cs} is the cross section area of the gauge section.

Including dwell times in LCF tests is possible. This is commonly used to study the short-time creep behaviour and creep-fatigue interactions at high temperatures [27, 65–67]. The dwell region can be established by either holding the stress or the total strain constant. This region is generally introduced for each cycle at the maximum load, the minimum load, or both. Holding the total strain constant at high temperatures produces stress relaxation, which is a form of creep behaviour. In each dwell region, the hold times are usually short, such as 5 minutes, to avoid extensive long tests. Isothermal LCF tests are usually run to failure by final rupture. However, several failure criteria can be used to obtain the final fatigue life, N_{f}, including stress-decrease criterion (see Sec. 3.3.1 and Fig. 3). Strain controlled isothermal LCF tests are well documented and described in several standards, e.g. see Ref. [48, 49].

In the study done by Azeez et al. [27] on the steam turbine steel FB2, isothermal LCF tests with and without dwell time were performed at several temperatures and total strain ranges, $\Delta\varepsilon_{\text{t}}$. All the tests are shown in Table 1 which were performed using the MTS servo-hydraulic rig in Fig. 11. The tests were done in strain control under fully reversed loading, $R_\varepsilon = -1$, with a constant strain rate of $\pm 10^{-3}$ 1/s. The tests were run to rupture, and the final fatigue life, N_{f}, was set based on stress-decrease fatigue criteria with 25 % drop in maximum stress. The time to failure, t_{f}, is also presented. The LCF tests with dwell were achieved by holding the total strain constant at both the maximum and the minimum load in each cycle. Each dwell region had 5 min hold time. The LCF tests were used to calibrate the material models needed for modelling the cyclic deformation behaviour of the steam turbine steel FB2. The tests with dwell time allowed the calibration of the creep model for this steam turbine steel. The mid-life hysteresis loops were obtained and used for fatigue life prediction following the strain-life approach (see Sec. 3.3.1).

4.1.1.1 Microstructural characterisation

The fracture surface of test specimens that have been run to rupture can be investigated. Microstructural characterisation of polished samples close to the fracture surface can also be of interest. This type of evaluation assists in understanding the material fatigue behaviour and the mechanisms behind the fatigue failure, especially at high temperatures.

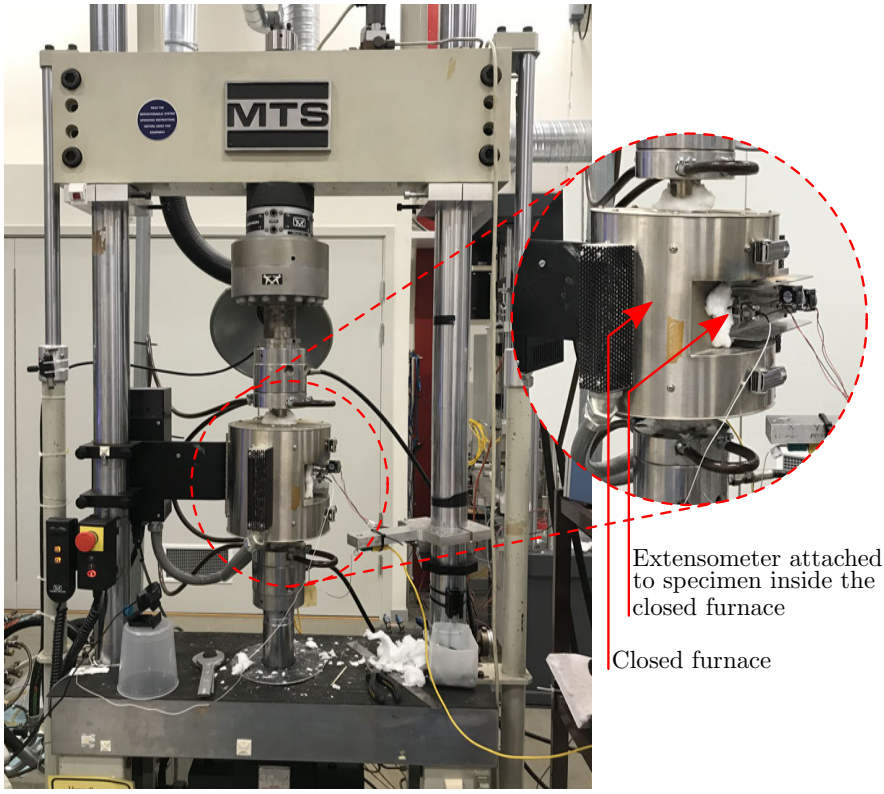

Figure 11: The MTS servo hydraulic test machine rig used for isothermal low cycle fatigue testing performed on steam turbine steel FB2 at Linköping University [27].

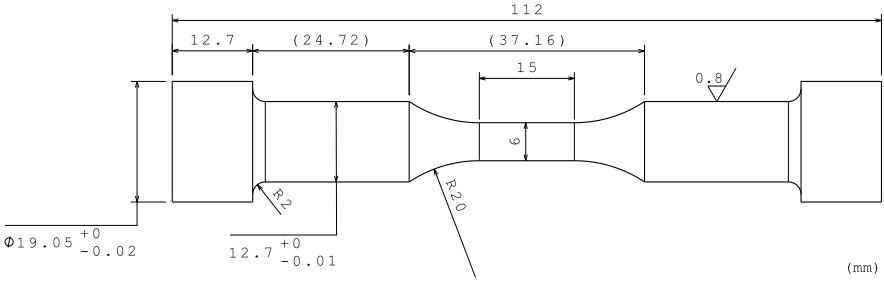

Figure 12: Detailed drawing of button head smooth cylindrical specimen used in isothermal low cycle fatigue testing on steam turbine steel FB2. Figure from Ref. [27].

Table 1: Performed isothermal LCF tests on steam turbine steel FB2. Table from Ref. [27]

Temperature, °C	$\Delta\varepsilon_t$, %	Dwell time, min	No. tests	N_f, Cycles	t_f, h
20	0.6	-	1	8910	29.70
20	0.8	-	1	4224	18.77
20	1.2	-	1	1820	12.13
400	0.8	-	1	2735	12.15
400	1.2	-	1	1349	8.99
500	0.8	-	2	2714; 3111	12.06; 13.82
500	1.2	-	1	807	5.38
600	0.8	-	2	1344; 1360	5.97; 6.04
600	1.2	-	1	789	5.26
500	0.8	5	1	1860	318.26
550	0.8	5	1	1580	270.35
600	0.8	5	1	870	148.86
625	0.8	5	1	730	124.91

In LCF testing done on the steam turbine steel FB2 [27], the crack initiation zone was determined by fractography. Then the gauge section was cut in half along the axial direction, x-axis, as illustrated in Fig. 13. The specimen was then mounted, and the cut surface was polished to allow the inspection of the microstructure directly below and away from the fracture surface. A Hitachi SU-70 field emission gun scanning electron microscope (SEM) was used for the microstructural investigations. Electron channelling contrast imaging (ECCI) technique of SEM along with electron backscatter diffraction (EBSD) were utilised to investigate the microstructure. Further details on the microstructure investigation carried on the steam turbine steel FB2 are available in Ref. [27].

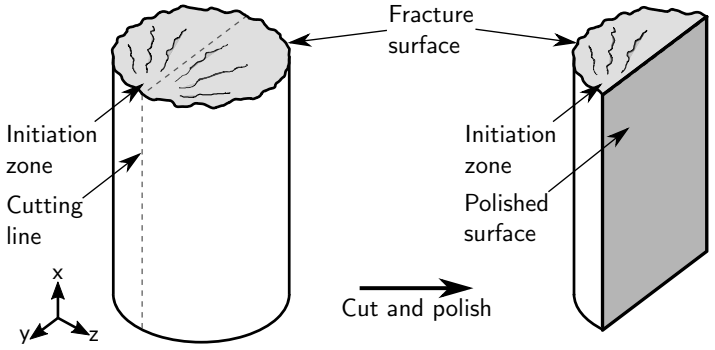

Figure 13: Schematic illustration of the sample preparation process done on the specimen gauge section after rupture. Microstructure investigation was performed on the polished surface. Figure from Ref. [27].

4.1.2 Isothermal fatigue crack propagation

Isothermal fatigue crack propagation tests have been widely used to investigate fatigue crack growth behaviour. The testing is generally done under force control with constant amplitude cyclic loading and constant load ratio. Compact tension (CT) specimen can be used for such testing. An isoparametric view of a CT specimen is illustrated in Fig. 14 a), where W is the effective width, B is the thickness, and a is the crack length measured from the load line. Pre-cracking is usually done before the actual testing to establish a sharp crack tip ahead of a machined crack starter. The pre-cracking procedure is generally run under low stress intensity ranges, ΔK [30]. The data obtained from fatigue crack propagation tests can be used to establish fatigue crack growth behaviour following the fracture mechanics approach (see Sec. 3.3.2). The test results are usually crack length, a, and the number of cycles, N, run until failure. There are several methods used for measuring the crack length during the test. Methods such as potential drop or compliance can be used. The data is typically processed to produce crack growth rate, $\mathrm{d}a/\mathrm{d}N$, versus stress intensity range, ΔK, and plotted using Paris law, Eq.7. Isothermal fatigue crack propagation testing is well documented, and several standards are available, e.g. Ref. [54, 68]. The determination of crack growth rate, $\mathrm{d}a/\mathrm{d}N$, from a versus N can be done following the recommended methods available in Ref. [68]. Furthermore, the stress intensity factor, K, equation for many specimen geometries are readily available in many handbooks and standards, e.g. Ref. [68]. For CT specimen, K can be defined as

$$K = \frac{F}{B\sqrt{W}} f_{\mathrm{CT}}\left(\frac{a}{W}\right) \tag{13}$$

where F is the applied load and f_{CT} is the stress intensity factor function for CT specimen provided by

$$f_{\mathrm{CT}}\left(\frac{a}{W}\right) = \frac{\left(2+\frac{a}{W}\right)}{\left(1-\frac{a}{W}\right)^{3/2}}\left(0.886 + 4.64\left(\frac{a}{W}\right) - 13.32\left(\frac{a}{W}\right)^2 + 14.72\left(\frac{a}{W}\right)^3 - 5.6\left(\frac{a}{W}\right)^4\right). \tag{14}$$

In the study done on the steam turbine steel FB2, isothermal crack growth test at 100 °C was performed using CT specimen with detailed drawing shown in Fig. 14 b) [26]. The testing set up used 100 kN Alwetron electro-mechanical test machine with an external digital controller Doli 580 V and a 3-zone split furnace as shown in Fig. 15. The specimen pre-cracking was carried at room temperature. The crack length measurement was done using pulsed direct-current potential drop system from Matelect with a current of 5 A and pulse frequency of 1 Hz. A standard procedure, described in Ref. [69], was followed to obtain crack length, a, from voltage for the CT specimen. The test was done using a load ratio of 0.05 and a load range of 4.5 kN.

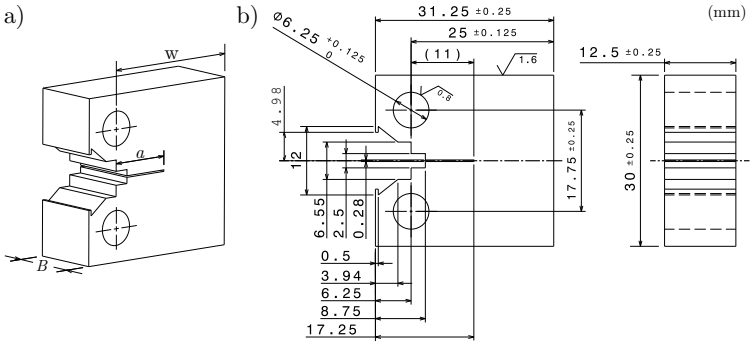

Figure 14: Compact tension specimen used for isothermal crack propagation testing on steam turbine steel FB2. (a) isoparametric view showing the effective width, W, thickness, B, and crack length, a; (b) detailed drawing. Figure from Ref. [26].

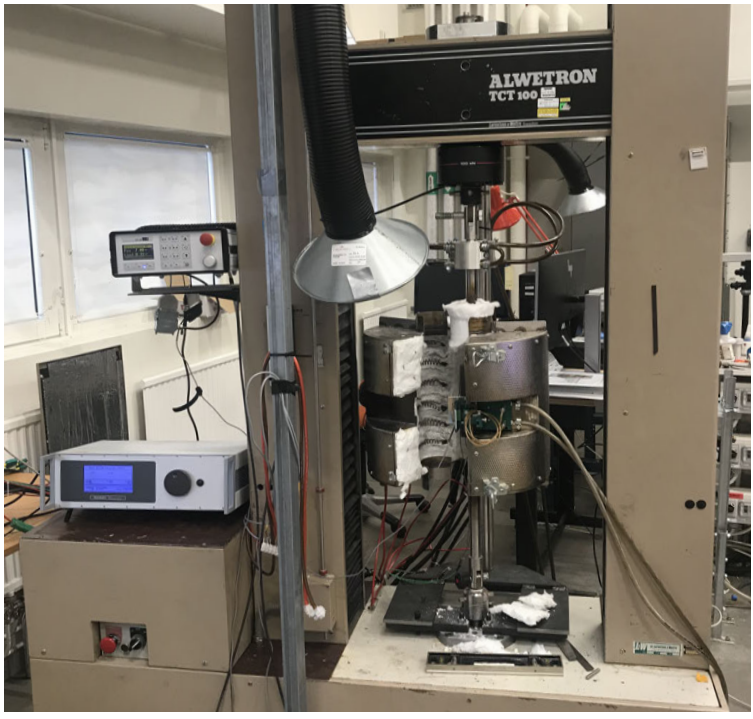

Figure 15: The Alwetron electro-mechanical test machine rig used for isothermal fatigue crack propagation testing performed on steam turbine steel FB2 at Linköping University [26].

4.1.3 Thermomechanical fatigue crack propagation

Thermomechanical fatigue crack propagation testing is generally more complicated in testing procedures and data post-processing than the isothermal fatigue crack propagation testing. Nonetheless, this kind of testing can be essential for studying fatigue crack growth behaviour of critical components where the temperature and the load vary largely over time, e.g. high-temperature steam turbine components. Thus, several researchers dedicated to investigating and providing guidelines for TMF crack growth testing [70–72]. Even though several standards are available for strain-control TMF testing on smooth specimens, e.g. Ref. [50, 73], TMF crack propagation testing still lacks standardisation. Nevertheless, experience and recommendations can still be exchanged between the two, as both types of testing utilise similar setup.

Different types of TMF cycle can be constructed based on how the load and the temperature are varied with time. The two common types of TMF cycle are OP and in-phase (IP). Figure 16 (a) and (b) illustrate a single crack propagation cycle under OP-TMF and IP-TMF, respectively. In OP-TMF, the maximum load occur at the minimum temperature and vice versa, while in IP-TMF the maximum load occur at the maximum temperature and vice versa. The TMF crack propagation testing discussed in this thesis defines the loading curve as causing the crack to open and the unloading curve as causing the crack to close, see Fig. 16. The choice of the TMF cycle depends mainly on the target component being investigated. An OP-TMF cycle is most relevant for investigation fatigue crack growth at the inner surface of the high-temperature inner casing of steam turbine, see Fig. 2.

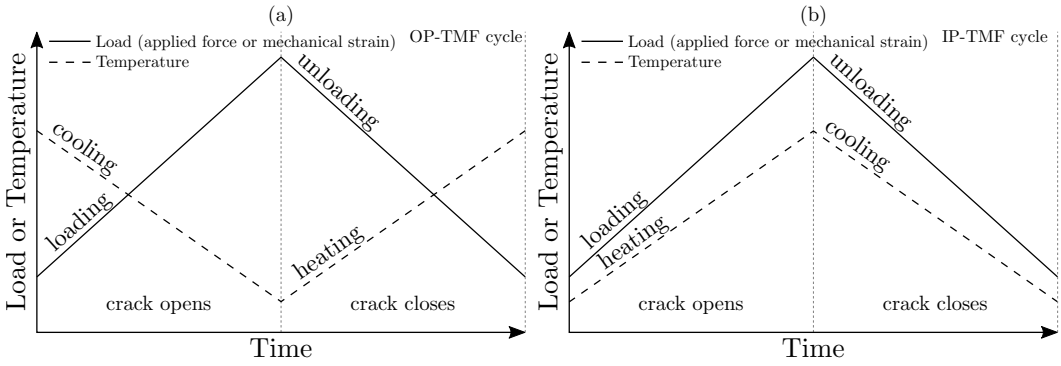

Figure 16: Schematic illustration of a single crack propagation cycle under (a) out-of-phase thermomechanical fatigue, OP-TMF, Fig. from Ref.[26]; (b) in-phase thermomechanical fatigue, IP-TMF.

Before conducting actual TMF crack propagation tests, several procedures are carried out, including thermal profiling, elastic modulus measurement, pre-cracking, and pre-test. Thermal profiling ensures proper temperature distribution within the specimen and usually done at the beginning of each testing series. The

elastic modulus measurement procedure is carried on each test specimen before pre-cracking to obtain the uncracked stiffness, E_{uncrk}, at different temperatures. The uncracked stiffness, E_{uncrk}, is later used in the compliance methods for crack length and crack closure measurements. The pre-cracking is performed to establish a sharp crack of reasonable length and is usually done at room temperature under stress control cycle with low stress range and high frequency. The pre-test procedure is done at the beginning of each crack growth test and includes thermal stabilisation, thermal strain measurement, and validation. The actual crack growth testing can be performed in either stress or strain control. In stress control, the applied force, F, is controlled. In strain control, the mechanical strain, ε_{mec}, is controlled, which is defined as

$$\varepsilon_{\text{mec}} = \varepsilon_{\text{tot}} - \varepsilon_{\text{th}} \tag{15}$$

where ε_{tot} is the total strain measured by the extensometer, and ε_{th} is the thermal strain due to thermal expansion. The nominal stress, σ_{nom}, during the cycle can be defined using Eq. 12, where A_{cs} can be set as the unnotched and uncracked gauge cross section area of the specimen. Test interruptions, deliberate or unintentional, could occur and might require a restarting procedure and compensation for the permanent inelastic strain the specimen has endured. This inelastic strain can be affected by the presence of crack closure.

Single edge cracked or notched tension specimens are commonly used in TMF crack growth testing [53, 56, 62, 63, 70, 74–78]. Figure 17 shows single edge cracked (SET) specimen used in TMF crack growth testing of the steam turbine steel FB2 by [26]. The specimen has a narrow manufactured crack starter of length, l, which helps in the initiation of sharp crack during pre-cracking, see schematic view of detail B in Fig. 17. The crack length, a, is defined as the combined length of the sharp crack and the crack starter. The stress intensity factor, K, for the SET specimen can be found using Eq. 6 where the width is $W = 12$ mm and the geometrical factor for SET specimen, $f_{\text{geo,SET}}$, is defined in Ref. [26] as

$$\begin{aligned} f_{\text{geo,SET}}\left(\frac{a}{W}\right) &= 261.22\left(\frac{a}{W}\right)^7 - 772.7\left(\frac{a}{W}\right)^6 + 918.2\left(\frac{a}{W}\right)^5 \\ &\quad - 556.4\left(\frac{a}{W}\right)^4 + 180.51\left(\frac{a}{W}\right)^3 - 28.49\left(\frac{a}{W}\right)^2 + 2.692\left(\frac{a}{W}\right) + 1.12. \end{aligned} \tag{16}$$

Thus, K can be determined for any nominal stress, σ_{nom}, in the experimental cycle for which the crack length, a, is known. The definition of $f_{\text{geo,SET}}$ was obtained using linear elastic FE modelling of the SET specimen and crack remeshing tool [79, 80] as discussed in Ref. [26].

All TMF crack growth tests for the steam turbine steel FB2, including all testing procedures, were carried out using the test set up shown in Fig. 18 [26]. Instron 8801 servo-hydraulic test machine was utilised, which was equipped with an induction heating coil and three air cooling nozzles surrounding the specimen. Instron extensometer 2632-055 with 12.5 mm gauge length was positioned over the crack starter. Instron TMF software was used to carry out the testing procedures. During

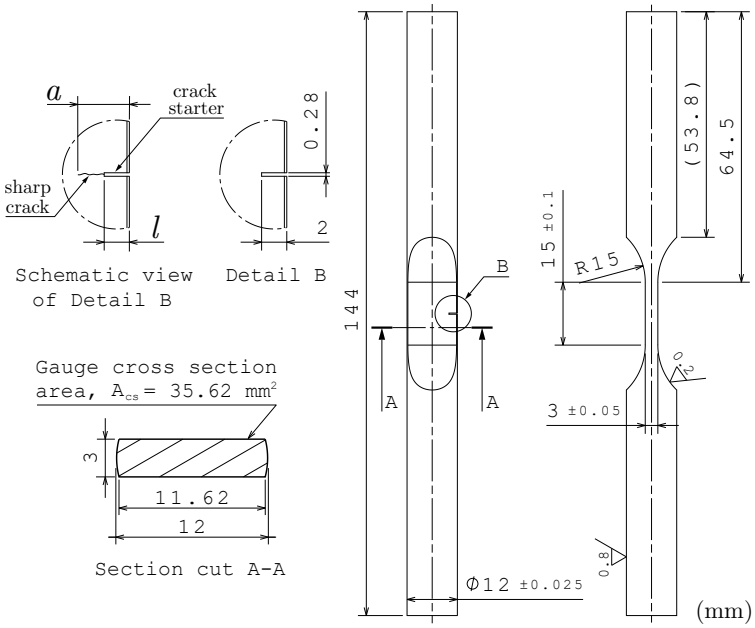

Figure 17: Single edge crack tension specimen used for thermomechanical fatigue crack propagation testing on steam turbine steel FB2. Schematic view of detail B shows crack starter length, l, and crack length, a. The section cut A-A shows the gauge cross section without sharp crack and crack starter. Figure from Ref. [26].

testing, the specimen's temperature was monitored using N-type thermocouples spot welded to the gauge section. However, during thermal profiling, six different N-type thermocouples were used, three on each side of the gauge section with even spacing along the axial direction. The heating coil and the cooling airflow were calibrated to achieve a uniform temperature distribution of less than 10 °C through the temperature cycle, as recommended by Ref. [50, 73]. Table 2 shows the OP-TMF crack growth tests performed on the steam turbine steel FB2, in the study done by Azeez et al. [26]. For stress controlled tests, $\Delta\sigma$ is the stress range and $R_\sigma = \sigma_{\min}/\sigma_{\max}$ is the stress ratio; $\sigma_{\min}$ and $\sigma_{\max}$ being the minimum and maximum stresses during the cycle. For strain controlled tests, $\Delta\varepsilon_{\text{mec}}$ is the mechanical strain range and R_ε is the strain ratio. All tests were run with the same maximum and minimum temperatures, $T_{\max} = 600$ °C and $T_{\min} = 100$ °C, respectively. Some tests were interrupted and restarted. For SET-01, the interruptions were deliberate to increase $\Delta\sigma$ and the restarting was successful. For SET-02, the interruption was unintentional, and the restarting was not completely successful as it led to an altered R_ε. The cooling and heating rates were constant for all tests with 5 °C/s leading to a cycle length of 200 s/cycle.

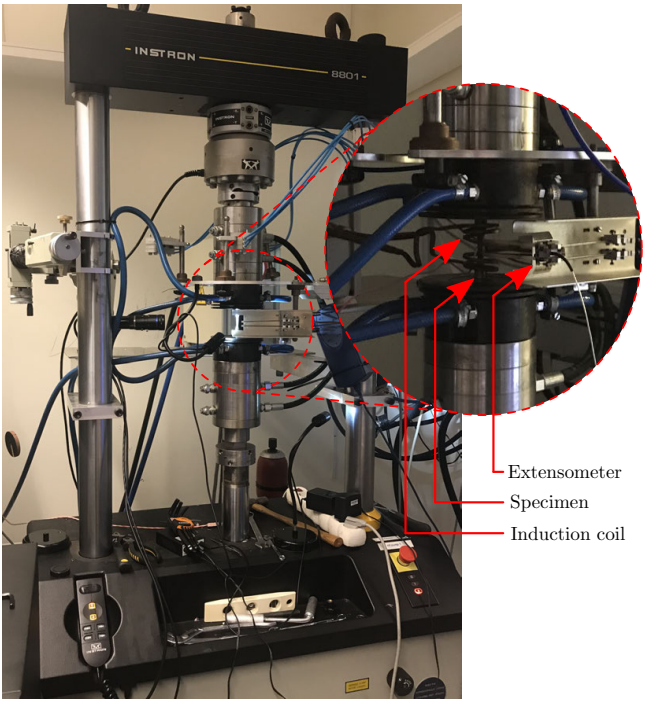

Figure 18: The Instron 8801 servo hydraulic test machine rig used for thermomechanical fatigue crack propagation testing performed on steam turbine steel FB2 at Linköping University [26]. Figure from Ref. [26].

Table 2: Out-of-phase thermomechanical fatigue crack propagation tests performed on steam turbine steel FB2. Table from Ref. [26].

Specimen	$T_{\min}$, °C	$T_{\max}$, °C	control	R_σ	R_ε	$\Delta\sigma$, MPa	$\Delta\varepsilon_{\text{mec}}$, %	l, mm	status
SET-01	100	600	Stress	0		200		2.13	Interrupted and restarted
	100	600	Stress	0		250			Interrupted and restarted
	100	600	Stress	0		300			Stopped
SET-02	100	600	Strain		$-\infty$		0.5	2.12	Interrupted and restarted
	100	600	Strain		≈-11		0.5		Stopped
SET-03	100	600	Strain		$-\infty$		0.5	2.22	Stopped
SET-04	100	600	Strain		$-\infty$		0.6	2.20	Stopped
SET-05	100	600	Strain		$-\infty$		0.6	2.14	Stopped
SET-06	100	600	Strain		$-\infty$		0.6	2.04	Stopped
SET-07	100	600	Strain		$-\infty$		0.7	2.21	Stopped

4.1.3.1 Crack length measurement method

Several methods have been reported in the literature for measuring the crack length extension during TMF testing. The lack of standardisation for TMF crack growth testing has motivated researchers to adapt methods recommended by isothermal crack growth standards, e.g. Ref. [54]. However, modifications must be done to account for the change in temperature due to TMF conditions. A code of practice for TMF crack growth testing by Stekovic et al. [70] has reported three different crack length measurement methods adapted for TMF conditions. Those methods were direct current potential drop (DCPD) method, alternating current potential drop (ACPD) method, and compliance method. A literature overview shows the use of such crack length measurement methods by researchers. The use of DCPD methods have been reported in Ref. [71, 72, 81–83] while the use of compliance methods have been seen in studies by Ref. [53, 56, 62, 63, 74–78]. A study in Ref. [84] has used the ACPD method. Optical methods for crack length measurements have also been utilised [85, 86]. However, due to resolution issues and limitation of crack measurements to the specimen's outer surface, other methods such as compliance methods and potential drop methods are more desirable. Unsymmetrical crack growth or crack tunnelling effects can also influence the optical measurements methods.

The potential drop methods give the ability for detailed monitoring of crack extension during a fatigue cycle, while the compliance method is limited to providing crack length measurement per cycle. This allows the potential drop method to analyse the crack growth process and mechanisms [87]. However, the induction coil system for TMF crack growth testing can create noise for the potential drop methods as induction can interfere with current [71]. Thus, compliance methods are recommended for TMF crack growth use. Furthermore, the compliance method requires less complicated testing setup than the potential drop method. Potential drop methods will not be further discussed here.

The compliance method used for TMF crack propagation work done on the steam turbine steel FB2 by [26] is discussed in detailed. Compliance method for crack length measurement, in general, utilises the concept that a change in the crack length, a, during testing produces a change in the normalised specimen stiffness, E_{norm}. Figure 19 shows a flowchart schematically illustrating the crack length measurement method in detail. Box 3 in the flowchart present the experimental crack length, a, computed using

$$a = g(E_{\text{norm}}) \tag{17}$$

where E_{norm} is the normalised specimen stiffness obtained from the experimental test, Box 1 of the flowchart in Fig. 19. The function, g, that describes the relation between E_{nom} and a is obtained through FE modelling, see Box 2 of the flowchart in Fig. 19.

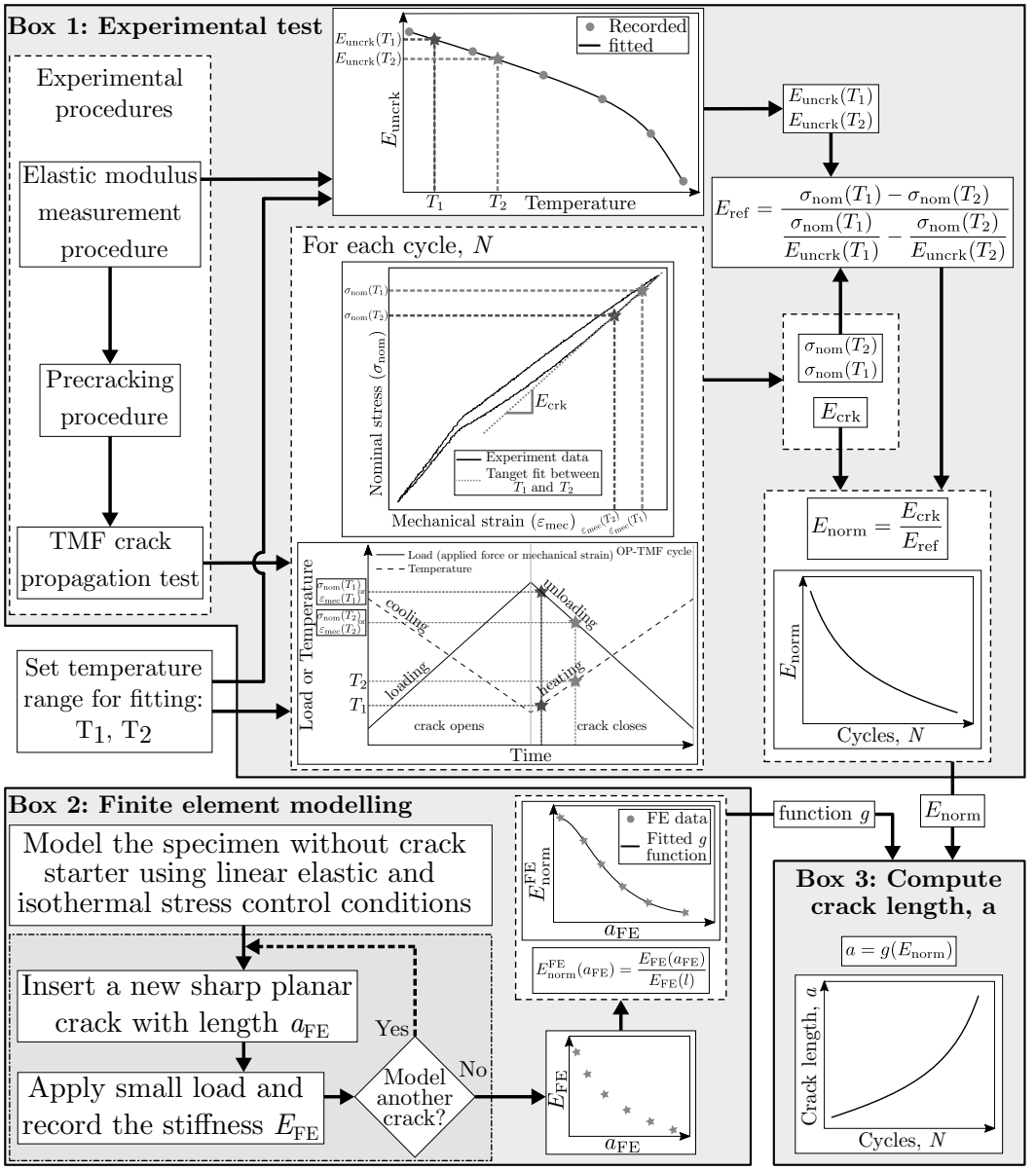

Figure 19: Flowchart showing the compliance-based crack length measurement method used in thermomechanical fatigue crack growth testing on the steam turbine steel FB2 done in Ref. [26].

The normalised stiffness, E_{nom}, is computed using

$$E_{\text{norm}} = \frac{E_{\text{crk}}}{E_{\text{ref}}} \tag{18}$$

where E_{crk} is the cracked specimen stiffness and E_{crk} is the reference stiffness. For each experimental TMF crack growth cycle, E_{crk} is set to be the slope of a straight line fitting within the elastic unloading interval of the σ_{nom}–ε_{mec} curve (see Box 1 in Fig. 19). The elastic unloading interval is set to be between $T_1 = 125$ °C and $T_2 = 225$ °C. The reference stiffness, E_{ref} is determined from

$$E_{\text{ref}} = \frac{\sigma_{\text{nom}}(T_1) - \sigma_{\text{nom}}(T_2)}{\frac{\sigma_{\text{nom}}(T_1)}{E_{\text{uncrk}}(T_1)} - \frac{\sigma_{\text{nom}}(T_2)}{E_{\text{uncrk}}(T_2)}} \tag{19}$$

where σ_{nom} and E_{uncrk} are the nominal stress and the uncracked specimen stiffness, respectively, at T_1 and T_2. The elastic modulus measurement procedure (discussed in Sec. 4.1.3) done before pre-cracking is used to determined E_{uncrk} at T_1 and T_2, see Box 1 in Fig. 19. In this thesis work, an uncracked SET specimen does not have a sharp crack yet it has a crack starter, see Fig. 17.

The function g is obtained from linear elastic FE model of the SET specimen without a crack starter. The FE software, ABAQUS [80], can be used to build the model. The boundary conditions applied are discussed in Ref. [26]. The elastic modulus was set to an arbitrary value of 200 GPa. Isothermal stress control loading conditions were used with $R_\sigma = 0$ and a stress range of $\Delta\sigma = 10$ kPa. Furthermore, a through-thickness sharp planar crack with length, a_{FE}, measured from the outer curvature (same as the definition of crack length, a, in the schematic view of detail B in Fig. 17) is inserted between the extensometer positions. The loading cycle is applied and the FE model stiffness, E_{FE}, is found from the slope of the modelled σ_{nom}–ε_{mec} curve. As multiple FE models with different sharp crack lengths were created, a description of E_{FE} versus a_{FE} can be obtained, see Box 2 in Fig. 19. An FE crack meshing software, such as Franc3D [79], can be used to insert and mesh sharp cracks. Moreover, an FE normalised stiffness as a function of the FE crack length, $E^{\text{FE}}_{\text{norm}}(a_{\text{FE}})$, can be obtained using

$$E^{\text{FE}}_{\text{norm}}(a_{\text{FE}}) = \frac{E_{\text{FE}}(a_{\text{FE}})}{E_{\text{FE}}(l)} \tag{20}$$

where $E_{\text{FE}}(a_{\text{FE}})$ is the FE model stiffness as a function of the FE crack length and $E_{\text{FE}}(l)$ is the FE model stiffness at FE crack length equal to the crack starter length, l (see Box 2 in Fig. 19). By fitting $E^{\text{FE}}_{\text{norm}}$ as a function of a_{FE}, the function g is obtained. It must be noted that the crack starter length, l, can be unique to the tested specimen. Thus, a unique function g can be obtained for each specimen.

4.1.3.2 Crack closure measurement method

Crack closure behaviour discussed in Sec. 3.3.2.1 can be accounted for by determining the stress or force level at which crack closure occurs. This allow the use of effective

stress intensity range defined in Eq. 10 and Eq. 11 to collapse the fatigue crack growth curves together (see Fig 10). Several methods exist for determining the crack opening stress (or crack opening force) under isothermal fatigue crack growth conditions. Techniques such as potential drop, ultrasonics, acoustic emission, eddy current, optical, and compliance can be used [54]. However, the less complicated experimental setup required for compliance method has made it favourable and widely used. In this thesis, only the compliance method for crack closure measurement will be discussed in detail. As TMF crack growth testing on high-temperature steam turbine steel has revealed crack closure behaviour [26], a compliance method adapted for TMF conditions is considered.

A presence of macrocrack within a specimen would lead to a noticeable change in its stiffness depending on if the crack faces are in contact or not (see Fig. 9 (a)). Based on this concept, the compliance method adapted for change in temperature due to TMF was used [26, 62, 78]. The method was original developed to only predict the crack opening stress, σ_{op}, from the loading curve of the TMF cycle [62]. However, the method was extended to estimate the crack closing stress, σ_{cl}, from the unloading curve of the TMF cycle [26]. This was motivated as the effective closing stress intensity range, $K_{\text{eff,cl}}$, was found to better collapse the crack growth behaviour for the steam turbine steel FB2 (see Fig. 10) [26]. The method used by Azeez et al. [26] defines degree of crack opening, D_{op}, and degree of crack closing, D_{cl}. As the load increases during the loading curve of the TMF cycle, D_{op} goes from 0, crack being fully closed, to 1, crack being fully open. On the other hand, D_{cl} goes from 1 to 0 instead, during the unloading of the TMF cycle. By defining a limit for D_{op} and D_{cl} that represent a fully open crack, i.e. close to 1, opening nominal stress, σ_{op}, and closing nominal stress, σ_{cl}, respectively, can be produced. A value close to 1 for D_{cl} represent a crack that began to close but is still completely open. The degree of crack opening, D_{op}, can be defined as [62]

$$D_{\text{op}} = \frac{1 - \dfrac{E_{\text{ld}}}{E_{\text{ref}}}}{1 - E_{\text{norm}}} \tag{21}$$

and degree of crack closing, D_{op}, as [26]

$$D_{\text{cl}} = \frac{1 - \dfrac{E_{\text{unld}}}{E_{\text{ref}}}}{1 - E_{\text{norm}}} \tag{22}$$

where E_{ref} is the reference stiffness defined in Eq. 19 and E_{norm} is the normalised specimen stiffness obtained for each cycle from Eq. 18 and described in Box 1 of Fig. 19 flowchart. Furthermore, E_{ld} and E_{unld} are the tangent stiffnesses during the loading and the unloading curves, respectively. Figure 20 (a) shows how E_{ld} and E_{unld} are computed from each curve at 60 different stress points equally spaced along the nominal stress range. Each stress point, on the loading or the unloading curve, has an an overlapping interval of 5 % of the nominal stress range. Within each interval, a tangent line is fitted on the σ_{nom}–ε_{mec} using least-square method to obtain E_{ld} and

E_{unld} on the loading and the unloading curve, respectively, as shown in Fig. 20 (a). The reference stiffness, E_{ref} is also computed for each interval using Eq. 19 where T_1 and T_2 are set to be the minimum and maximum temperatures within the interval. A unique value for E_{ld}, E_{unld} and E_{ref} is determined for each stress point on the loading and the unloading curve to produce D_{op} and D_{cl}, respectively, for each cycle as shown in Fig 20 (b). Using a level of D_{op} and D_{cl} equal to 0.9, the crack opening stress, σ_{op}, and crack closing stress, σ_{cl}, can be found for each TMF cycle, see Fig 20 (b). The choice of higher D_{op} and D_{cl} levels would increase the scatter and complicate the evaluation of short crack lengths. The use of level close or equal to 0.9 have also been documented by other researchers [62, 63, 78].

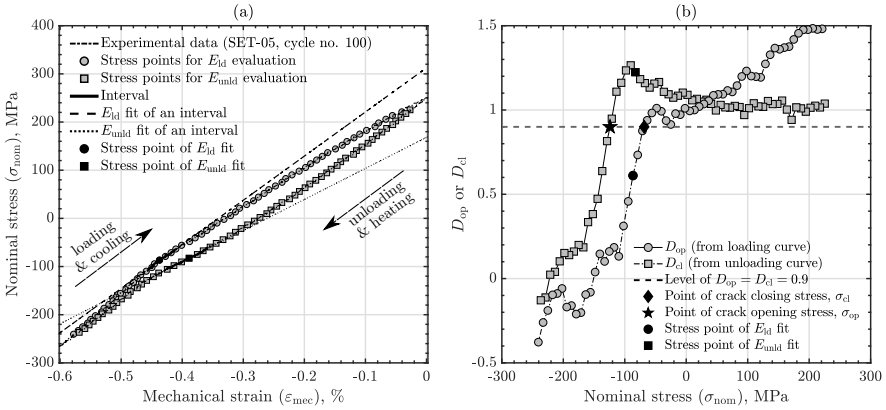

Figure 20: Compliance based crack closure measurement method applied on an OP-TMF cycle, where (a) shows the stress points of the loading and unloading curves used for computing E_{ld} and E_{un}, respectively; and (b) shows D_{op} and D_{cl} for a single cycle with level of 0.9 to produce crack opening stress, σ_{op}, and crack closing stress, σ_{op}. Figure from Ref. [26].

4.2 Material models and mechanical properties

Material models are necessary to simulate the deformation behaviour of a material. Finite element method is generally used to simulate and estimate material deformations behaviour. Several constitutive material models can be available as a built-in routine in an FE software, such as Abaqus [80]. However, some models might need to be implemented by the user. Material models require calibrated mechanical properties extracted from the actual material behaviour. This is usually obtained from experimental testing of specimens made from the same material. Isotropic behaviour is commonly observed for polycrystalline materials, such as the steam turbine steel FB2, where the mechanical properties are assumed identical in all directions [26, 27]. Other materials, such as single crystals and additively

manufactured materials, can present anisotropic behaviour, implying dependency of mechanical properties on the loading direction [88–91].

For the steam turbine steel FB2, the cyclic deformation behaviour was numerically simulated using a combined elasto-plastic material model and creep material model, see Ref. [26, 27]. These models were provided by the FE software, Abaqus [80], as built-in constitutive models where plasticity and creep were uncoupled. This modelling approach was considered usable as the numerical results reproduced the experimental cycles with acceptable accuracy [26, 27]. The elasto-plastic model used consisted of a linear elastic model and nonlinear kinematic hardening model with two back-stresses. Associated flow rule with von Mises yield criteria was utilised. The hardening model evolution law contains the Ziegler's kinematic law plus a recall term for each of the back-stresses, $\boldsymbol{\alpha}_m$, [80]

$$\dot{\boldsymbol{\alpha}}_m = C_m \frac{\boldsymbol{\sigma} - \boldsymbol{\alpha}}{\sigma_y} \dot{\bar{\varepsilon}}^{\mathrm{p}} - \gamma_m \boldsymbol{\alpha}_m \dot{\bar{\varepsilon}}^{\mathrm{p}} \tag{23}$$

and the total back-stress tensor is

$$\boldsymbol{\alpha} = \sum_{m=1}^{2} \boldsymbol{\alpha}_m \tag{24}$$

where C_m and γ_m are temperature dependent material parameters with $m = 1, 2$, while $\dot{\boldsymbol{\alpha}}_m$, $\boldsymbol{\sigma}$, σ_y, and $\dot{\bar{\varepsilon}}^{\mathrm{p}}$ are the rate of the back-stress tensor, the stress tensor, the yield strength, and the equivalent plastic strain rate, respectively. The creep model consists of a Norton power law defined as [92]

$$\dot{\bar{\varepsilon}}^{\mathrm{c}} = A \tilde{\sigma}^n \tag{25}$$

where $\dot{\bar{\varepsilon}}^{\mathrm{c}}$ and $\tilde{\sigma}$ are the equivalent creep strain rate and the equivalent stress, respectively, while A and n are temperature dependent fitted material parameters. All the mechanical properties used to calibrate the material models for the steam turbine steel FB2 were extracted from the isothermal LCF testing (see Sec. 4.1.1).

For the linear elastic model, Table 3 shows the temperature-dependent elastic properties of FB2, where E is the elastic modulus, and nu is the Poisson's ratio. The monotonic loadings of the first half-cycle for all isothermal LCF tests with and without dwell times were used to determine the average elastic modulus, E, at each temperature.

Table 3: Linear elastic temperature dependent material properties of the steam turbine steel FB2. Data from Ref. [26].

Temperature, °C	E, GPa	ν
20	213.97	0.285
400	186.69	0.299
500	179.91	0.305
550	170.24	0.308
600	159.41	0.312
625	147.36	0.314

For the nonlinear kinematic hardening model, Table 4 present the temperature-dependent parameters of FB2 used for modelling the plastic behaviour of the initial cycles and the mid-life cycles. Only LCF tests without dwell were used for the calibration of the plastic parameters. For the initial cyclic behaviour, the parameters were fitted from the monotonic loading of the first half-cycle. For the mid-life cyclic behaviour, the parameters were fitted from the loading curve of the mid-life cycle. The applied total mechanical strain range, $\Delta\varepsilon_t$, with the temperature, in Table 4, indicate from which LCF test the fitting parameters were extracted (see Table 1).

Table 4: The temperature dependent material parameters for the nonlinear kinematic hardening model used to model the initial and the mid-life cyclic plastic behaviour of the steam turbine steel FB2. Data from Ref. [27] and Ref. [26].

Modelling behaviour	Temperature, °C	$\Delta\varepsilon_t$, %	σ_y, MPa	C_1, MPa	C_2, MPa	γ_1	γ_2
Initial cycles							
	20	2.0	588.40	44680	322985	426.07	4157.7
	400	1.2	481.22	85958	229111	828.84	5821.7
	500	1.2	420.31	101264	257438	870.96	5782.6
	600	1.2	300.20	118360	584880	1056.4	7054.7
Mid-life cycles							
	20	0.6	300.05	1019030	538798	11996	1491
	20	0.8	282.12	534110	197090	4509.3	576.46
	20	1.2	308.24	90470	328880	332.96	2687.6
	400	0.8	234.12	125930	488520	502.79	5315.1
	400	1.2	218.91	408060	71678	3645.8	352.18
	500	0.8	197.11	91938	331860	430.63	4014.5
	400	1.2	195.36	52327	374730	322.62	3179.9
	600	0.8	154.06	82488	504880	562.3	7661.1
	600	1.2	151.32	34626	251620	266.26	3054.1

For the creep model, Table 5 shows the temperature-dependent parameters of FB2 used for modelling the creep behaviour in the initial cycles and the mid-life cycles. The hold time region of the LCF tests with dwell was used to calibrate the creep parameters. Due to the isotropic behaviour of the creep in tension and compression, only the dwell region in tension was considered. For the initial cycles, average creep parameters, A and n, were extracted from first few cycles (2–5 cycles) at each temperature. For mid-life cycles, average creep parameters within 20–80 % of the fatigue life were taken at each temperature. However, the mid-life creep parameters at 500 °C were taken from a cycle with less creep. For both initial and mid-life parameters, A was fitted using the Arrhenius equation and n using 2nd degree polynomial. Those fits were then used to obtain the data presented in Table 5. The fitting procedure of the creep parameters is explained in Ref. [27].

Table 5: The temperature dependent material parameters for the creep model used to model the initial and the mid-life cyclic creep behaviour of the steam turbine steel FB2. Data from Ref. [27] and Ref. [26].

Modelling behaviour	Temperature, °C	A, $1/(\mathrm{GPa}^n \cdot \mathrm{s})$	n
Initial cycles			
	500	6.65×10^4	30.27
	550	8.10×10^2	19.95
	600	16.37	13.69
	625	16.37	12.08
Mid-life cycles			
	500	4.55×10^{13}	43.04
	550	1.84×10^9	26.80
	600	1.54×10^5	15.96
	625	2.08×10^3	12.55

4.3 Modelling of crack closure

Numerical modelling has been widely used to explain and predict crack closure phenomenon [59, 60]. Finite element method is commonly used to study plasticity induced crack closure. Modelling by FE is desirable as full fields of stress and strain can be obtained. Also, the parameters that affect crack closure can be explored [59, 93]. Two dimensional FE models have been mostly used to investigate crack closure under both plane strain and plane stress conditions [56, 63, 64, 94, 95]. Studies on crack closure using three dimensional FE models were also seen [26, 96–98]. However, due to higher computational cost and modelling challenges associated with three-dimensional problems, more work has been done using two-dimensional models. Difficulties associated with FE modelling such as element type, mesh refinement, crack tip node release scheme, geometrical effects, crack closure assessment techniques are among the studied topics [60, 61, 99] Strip yield models based on Dugdale [100] work have also been considered for investigating plasticity induced crack closure [101–104]. Recent studies have been investigating modelling of crack closure under TMF conditions [26, 56, 63, 103].

The crack closure behaviour observed for the steam turbine steel FB2 tested under OP-TMF crack growth was predicted using a three dimensional FE model of the SET specimen [26]. The FE model uses sharp stationary crack with contacts conditions at the crack surfaces to avoid interpenetration during compressive loading. Elasto-plastic and creep material models for initial cycles behaviour of FB2 were utilised, see Sec. 4.2. A detailed description of the FE model, including the applied boundary conditions, loading, and mesh, along with the model's verification, is presented in Ref. [26]. For each test, where crack closure was observed, several FE models were built with different crack lengths. The simulations were run for five cycles. From the 5th cycle for each model, the crack closure measurement method adapted for TMF conditions (see Sec. 4.1.3.2) was applied on the modelled

σ_{nom}–ε_{mec} curve. The crack opening stress, σ_{op} was obtained from the loading curve and the crack closing stress, σ_{cl}, was obtained from the unloading curve. Figure 21 shows the crack closure stresses (σ_{op} and σ_{cl}) obtained from the modelled and the experimental cycles for the OP-TMF tests (see Table 2) with crack closure. A reasonable accuracy can be observed from the modelled crack closure stresses compare to the experimental ones, especially for short crack length, a. The FE model lacks the ability to capture the relaxation of the minimum stress over cycles for long crack lengths. This could be a reason behind the better prediction of crack closure stresses at short crack lengths compared to long crack lengths. Using the effective stress intensity ranges definition, in Eq. 10 for opening stresses and Eq. 11 for closing stresses, the modelled crack closure stresses can be used to construct the fatigue crack growth behaviour. Figure 22 shows the crack growth rate versus the FE effective stress intensity ranges obtained using the crack closure stresses. Comparing to Fig. 8 and Fig. 10, the use of crack closure stresses from an FE model with stationary crack seems to collapse the curves together using both the FE effective opening stress intensity range, $\Delta K_{\text{eff,op}}$ in Fig. 22 (a) and the FE effective closing stress intensity range, $\Delta K_{\text{eff,cl}}$ in Fig. 22 (b). Similar to accounting for crack closure experimentally, the use FE $\Delta K_{\text{eff,cl}}$ seems to align the crack growth curves better with the stress-controlled OP-TMF tests (SET-01) and the isothermal crack propagation test at 100 °C (see Fig. 10).

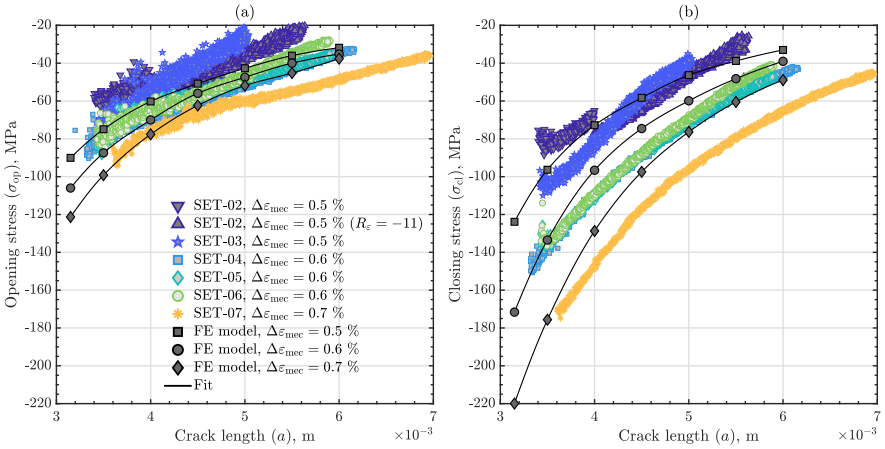

Figure 21: Crack closure levels obtained from experimental and numerical ccycles as a function of crack length, a, using (a) crack opening stress, σ_{op}; (b) crack closing stress, σ_{cl}. Figure from Ref. [26].

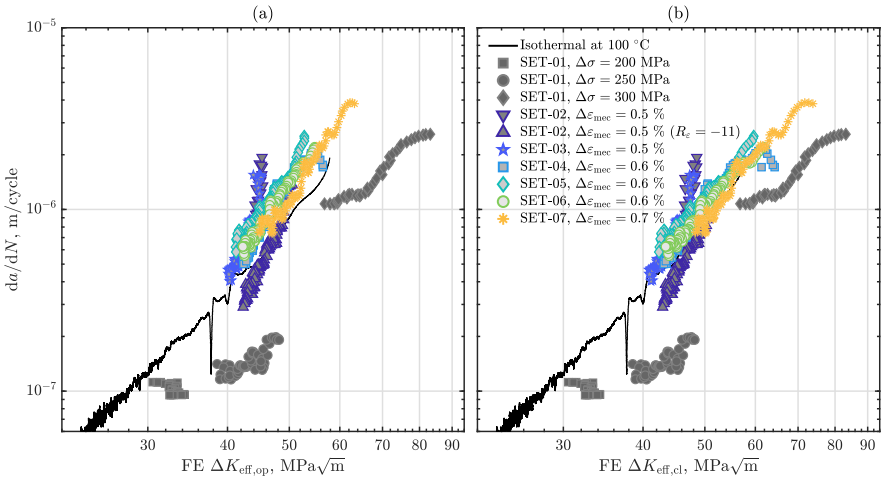

Figure 22: Crack growth rate, da/dN, versus FE effective stress intensity range using (a) FE effective opening stress intensity range, $\Delta K_{eff,op}$; (b) FE effective closing stress intensity range, $\Delta K_{eff,cl}$. Figure from Ref. [26].

5 Summary of Appended Papers

Paper I

Low cycle fatigue life modelling using finite element strain range partitioning for a steam turbine rotor steel

This paper investigates the steam turbine steel FB2 behaviour under LCF conditions where some tests included hold times. Mechanical properties including elastic, plastic and creep properties were captured. Microstructure investigations were carried out to investigate the effect of high-temperature fatigue. Fatigue life models based on stress amplitude (Basquin), inelastic strain amplitude (Coffin-Manson), and total strain amplitude (Coffin-Manson-Basquin) were investigated and showed the inability to predict the fatigue life of FB2 for all temperatures. Finite element modelling of the mid-life hysteresis curve was done using both elasto-plastic and creep models. Motivated by strain range partitioning (SRP) approach, the FE model was used to split the inelastic strain amplitude, from the mid-life hysteresis cycles, into plastic strain amplitude and creep strain amplitude. This split allowed the construction of fatigue life models grouped based on temperature to plasticity dominated region, in terms of plastic strain amplitude, and creep dominated region, in terms of creep strain amplitude. Those models were based on the Coffin-Manson relation. The FE SRP approach was suitable for establishing a life prediction model based on the transition temperature where creep damage became the dominant factor in determining fatigue life. For FB2 steel, the transition was seen at 500 °C for high applied total strain range and above 500 °C for all applied strain ranges. Microstructural investigations on the regions below the fracture surface were done to determine the damage mechanisms during fatigue. At high temperatures, signs of creep damage were visible in terms of voids at the grain boundaries. The fraction of LAGBs was used to quantify the plastic deformation, indicating large part of the inelastic strain at high temperature could be creep strain.

Paper II

Out-of-phase thermomechanical fatigue crack propagation in a steam turbine steel — modelling of crack closure

This paper investigates fatigue crack growth behaviour of the steam turbine steel FB2 under both isothermal fatigue and TMF loading conditions. The TMF crack growth testing was done under OP cycle in both stress control and strain control with a temperature range of 100–600 °C. All TMF tests performed in strain control showed crack closure behaviour, which was indicated in the nominal stress versus mechanical strain curves as a visible change in the specimen's global stiffness below the zero nominal stress. Compliance method adapted for TMF conditions was used to measure the nominal stress at which the crack open during loading and the nominal stress at which the crack closes during unloading. A noticeable difference between the crack opening and crack closing stress was observed, especially for short cracks. Accounting for crack closure using the effective stress intensity range shows a clear collapse of the fatigue crack growth curves together within a short scatter band. The collapsed curves coincided with the isothermal fatigue crack growth test performed at the minimum temperature of the OP-TMF cycle, i.e. 100 °C. A better collapse of the curves occurred when accounting for crack closure using the crack closing stress. Furthermore, a three-dimensional FE model with a stationary crack and contacts conditions was used to predict crack closure behaviour successfully. Also, the FE effective stress intensity ranges were similar to the experimentally computed ones. The difference between crack opening stress and crack closing stress was explained using FE modelling.

6 Conclusion

The current research characterises fatigue life behaviour of a steam turbine material at high temperature and utilises FE modelling to predict the material behaviour. Isothermal LCF tests were used to model the cyclic deformation behaviour and construct a fatigue life based on plastic dominant and creep dominant regions. Crack propagations tests under isothermal fatigue and TMF conditions were used to investigate the fatigue crack growth behaviour. Crack closure behaviour was accounted for and predicted using FE modelling.

The modelling of cyclic deformation of a steam turbine steel was done using elasto-plastic and creep models. The material models were calibrated for both initial cyclic and stable cyclic behaviour. A splitting of the inelastic strain amplitude into plastic and creep components at the mid-life cycles was possible using FE modelling. A fatigue life model based on this splitting was constructed to characterise the high-temperature fatigue life of the steam turbine steel FB2. This life prediction model was based on the Coffin-Manson relation, where the plastic-dominant region was in terms of the plastic strain amplitude and the creep-dominant region was in terms of the creep strain amplitude. Microstructural investigations in support of this life prediction model revealed signs of creep damage in the form of voids at the grain boundaries at high temperature. Also, the quantification of LAGBs showed that at high temperatures, the inelastic strain amplitude was accompanied by a reduction in the LAGBs. This suggests that a significant part of the inelastic strain at high temperatures can be creep strain.

Crack propagation results under OP-TMF conditions showed a clear sign of crack closure for the steam turbine steel FB2. A crack closure measurement method adapted for temperature changes was used to determine the crack closure levels from the experimental nominal stress versus mechanical strain curves. The crack opening and the crack closing stresses were determined from the loading and the unloading curves, respectively. It was found that account for crack closure using the crack closing stress produces a better collapse of the fatigue crack growth curves. The collapsed curves coincided with an isothermal crack propagation test performed at the minimum temperature of the OP-TMF cycle. The crack closure behaviour was simulated using three dimensional FE model with a stationary crack and contact conditions.

References

[1] Enrico Sciubba. Turbines, steam. In Cutler J. Cleveland, editor, *Encyclopedia of Energy*, pages 231 – 254. Elsevier, New York, 2004. ISBN 978-0-12-176480-7. doi: https://doi.org/10.1016/B0-12-176480-X/00097-8.

[2] Lee S. Langston. Turbines, gas. In Cutler J. Cleveland, editor, *Encyclopedia of Energy*, pages 221 – 230. Elsevier, New York, 2004. ISBN 978-0-12-176480-7. doi: https://doi.org/10.1016/B0-12-176480-X/00098-X.

[3] T. Tanuma. 1 - introduction to steam turbines for power plants. In Tadashi Tanuma, editor, *Advances in Steam Turbines for Modern Power Plants*, pages 3 – 9. Woodhead Publishing, 2017. ISBN 978-0-08-100314-5. doi: https://doi.org/10.1016/B978-0-08-100314-5.00001-4.

[4] Rama S. R. Gorla and Aijaz A. Khan. *Turbomachinery : design and theory.* Mechanical engineering (Marcel Dekker, Inc.): 160. Marcel Dekker, 2003. ISBN 0824709802.

[5] Dipak K. Sarkar. Chapter 6 - steam turbines. In Dipak K. Sarkar, editor, *Thermal Power Plant*, pages 189 – 237. Elsevier, 2015. ISBN 978-0-12-801575-9. doi: https://doi.org/10.1016/B978-0-12-801575-9.00006-8.

[6] Heinz P. Bloch and Murari P. Singh. *Steam turbines: design, applications, and rerating.* McGraw-Hill's AccessEngineering. McGraw-Hill, second edition edition, 2009. ISBN 9780071508216.

[7] N. Okita, T. Takahashi, and K. Nishimura. 20 - steam turbines for solar thermal and other renewable energies. In Tadashi Tanuma, editor, *Advances in Steam Turbines for Modern Power Plants*, pages 487 – 500. Woodhead Publishing, 2017. ISBN 978-0-08-100314-5. doi: https://doi.org/10.1016/B978-0-08-100314-5.00020-8.

[8] A. Kumbhare, S. Chaturvedi, M. K. Puri, and R. Rathore. An electricity generation using solar power steam turbine. In *2018 International Conference on Advanced Computation and Telecommunication (ICACAT)*, pages 1–4, 2018. doi: 10.1109/ICACAT.2018.8933663.

[9] Torsten-Ulf Kern, Marc Staubli, and Brendon Scarlin. The European Efforts in Material Development for 650 °C USC Power Plants - COST522. *ISIJ International*, 42(12):1515–1519, 2002. doi: 10.2355/isijinternational.42.1515.

[10] N. Funahashi. 22 - steam turbine roles and necessary technologies for stabilization of the electricity grid in the renewable energy era. In Tadashi Tanuma, editor, *Advances in Steam Turbines for Modern Power Plants*, pages 521 – 537. Woodhead Publishing, 2017. ISBN 978-0-08-100314-5. doi: https://doi.org/10.1016/B978-0-08-100314-5.00022-1.

[11] Michael Wechsung, Andreas Feldmüller, Heiko Lemmen. Steam turbines for flexible load operation in the future market of power generation. In *Proceedings of the ASME Turbo Expo 2012: Turbine Technical Conference and Exposition. Volume 6: Oil and Gas Applications; Concentrating Solar Power Plants; Steam Turbines; Wind Energy*, pages 579–588, Copenhagen, Denmark, June 2012. ASME.

[12] M. Topel, R. Guédez, and B. Laumert. Impact of increasing steam turbine flexibility on the annual performance of a direct steam generation tower power plant. *Energy Procedia*, 69:1171 – 1180, 2015. ISSN 1876-6102. doi: https://doi.org/10.1016/j.egypro.2015.03.196. International Conference on Concentrating Solar Power and Chemical Energy Systems, SolarPACES 2014.

[13] Davide Ferruzza and Monika Topel and Björn Laumert and Fredrik Haglind. Impact of steam generator start-up limitations on the performance of a parabolic trough solar power plant. *Solar Energy*, 169:255 – 263, 2018. ISSN 0038-092X. doi: https://doi.org/10.1016/j.solener.2018.05.010.

[14] Peter Stein, Gabriel Marinescu, Dominik Born, Michael Lerch. Thermal modeling and mechanical integrity based design of a heat shield on a high pressure module solar steam turbine inner casing with focus on lifetime. In *Proceedings of the ASME Turbo Expo 2014: Turbine Technical Conference and Exposition. Volume 5C: Heat Transfer*, Düsseldorf, Germany, June 2014. ASME. doi: https://doi.org/10.1115/GT2014-25846.

[15] H. Nomoto. 21 - Advanced ultra-supercritical pressure (A-USC) steam turbines and their combination with carbon capture and storage systems (CCS). In Tadashi Tanuma, editor, *Advances in Steam Turbines for Modern Power Plants*, pages 501 – 519. Woodhead Publishing, 2017. ISBN 978-0-08-100314-5. doi: https://doi.org/10.1016/B978-0-08-100314-5.00021-X.

[16] I. McBean. 16 - manufacturing technologies for key steam turbine parts. In Tadashi Tanuma, editor, *Advances in Steam Turbines for Modern Power Plants*, pages 381 – 393. Woodhead Publishing, 2017. ISBN 978-0-08-100314-5. doi: https://doi.org/10.1016/B978-0-08-100314-5.00016-6.

[17] T U Kern, K H Mayer, B Donth, G Zeiler, and A Di Gianfrancesco. The European efforts in development of new high temperature rotor materials

- COST536. In *Proc. of 9th Liege Conf. on Materials for Advanced Power Engineering*, pages 27–36, Liege, Belgium, July 2010.

[18] Fujio Abe. Research and Development of Heat-Resistant Materials for Advanced USC Power Plants with Steam Temperatures of 700 ∘C and Above. *Engineering*, 1(2):211 – 224, 2015. ISSN 2095-8099. doi: https://doi.org/10.15302/J-ENG-2015031.

[19] S. Holdsworth. Creep resistant materials for steam turbines. In *Reference Module in Materials Science and Materials Engineering*. Elsevier, 2016. ISBN 978-0-12-803581-8. doi: https://doi.org/10.1016/B978-0-12-803581-8.02063-4.

[20] R. Mishnev, N. Dudova, and R. Kaibyshev. On the origin of the superior long-term creep resistance of a 10% Cr steel. *Materials Science and Engineering: A*, 713:161–173, 2018. ISSN 0921-5093. doi: https://doi.org/10.1016/j.msea.2017.12.066.

[21] H. Nomoto. 12 - Development in materials for ultra-supercritical (USC) and advanced ultra-supercritical (A-USC) steam turbines. In Tadashi Tanuma, editor, *Advances in Steam Turbines for Modern Power Plants*, pages 263–278. Woodhead Publishing, 2017. ISBN 978-0-08-100314-5. doi: https://doi.org/10.1016/B978-0-08-100314-5.00012-9.

[22] N. Lückemeyer, H. Kirchner, H. Almstedt. Challenges in Advanced-USC Steam Turbine Design for 1300°F / 700°C. In *roceedings of the ASME Turbo Expo 2012: Turbine Technical Conference and Exposition. Volume 6: Oil and Gas Applications; Concentrating Solar Power Plants; Steam Turbines; Wind Energy*, pages 685–693, Copenhagen, Denmark, June 2012. ASME.

[23] Guocai Chai, Magnus Boström, Magnus Olaison, and Urban Forsberg. Creep and LCF Behaviors of Newly Developed Advanced Heat Resistant Austenitic Stainless Steel for A-USC. *Procedia Engineering*, 55:232–239, 2013. ISSN 1877-7058. doi: https://doi.org/10.1016/j.proeng.2013.03.248. 6th International Conference on Creep, Fatigue and Creep-Fatigue Interaction.

[24] Hugo Wärner, Jinghao Xu, Guocai Chai, Johan Moverare, and Mattias Calmunger. Microstructural evolution during high temperature dwell-fatigue of austenitic stainless steels. *International Journal of Fatigue*, 143:105990, 2021. ISSN 0142-1123. doi: https://doi.org/10.1016/j.ijfatigue.2020.105990.

[25] G. Zeiler. 6 - martensitic steels for rotors in ultra-supercritical power plants. In Augusto Di Gianfrancesco, editor, *Materials for Ultra-Supercritical and Advanced Ultra-Supercritical Power Plants*, pages 143 – 174. Woodhead Publishing, 2017. ISBN 978-0-08-100552-1. doi: https://doi.org/10.1016/B978-0-08-100552-1.00006-3.

[26] Ahmed Azeez, Viktor Norman, Robert Eriksson, Daniel Leidermark, and Johan Moverare. Out-of-phase thermomechanical fatigue crack propagation

in a steam turbine steel — modelling of crack closure. *International Journal of Fatigue*. Conditionally accepted. (Appended to this licentiate thesis).

[27] Ahmed Azeez, Robert Eriksson, Daniel Leidermark, and Mattias Calmunger. Low cycle fatigue life modelling using finite element strain range partitioning for a steam turbine rotor steel. *Theoretical and Applied Fracture Mechanics*, Volume 107:Article 102510, 2020. ISSN 0167-8442. doi: https://doi.org/10.1016/j.tafmec.2020.102510. (Appended to this licentiate thesis).

[28] Yifeng Hu, Puning Jiang, Xingzhu Ye, Gang Chen, Junhui Zhang, Zhenzhen Hao, Lei Xiao. Lifetime assessment of steam turbine casing. In *Proceedings of the ASME Turbo Expo 2015: Turbine Technical Conference and Exposition. Volume 8: Microturbines, Turbochargers and Small Turbomachines; Steam Turbines*, Montreal, Quebec, Canada, June 2015. ASME. doi: https://doi.org/10.1115/GT2015-43495.

[29] S. Suresh. *Fatigue of Materials*. Cambridge University Press, 2 edition, 1998. doi: 10.1017/CBO9780511806575.

[30] Ralph I. Stephens, Ali Fatemi, Robert R. Stephens, and Henry O. Fuchs. *Metal Fatigue in Engineering*. John Wiley & Sons, INC., 2 edition, October 2000. ISBN 978-0-471-51059-8.

[31] Gerard Kosman and Andrzej Rusin. The influence of the start-ups and cyclic loads of steam turbines conducted according to european standards on the component's life. *Energy*, 26(12):1083 – 1099, 2001. ISSN 0360-5442. doi: https://doi.org/10.1016/S0360-5442(01)00071-8.

[32] Y. Enomoto. 17 - steam turbine retrofitting for the life extension of power plants. In Tadashi Tanuma, editor, *Advances in Steam Turbines for Modern Power Plants*, pages 397 – 436. Woodhead Publishing, 2017. ISBN 978-0-08-100314-5. doi: https://doi.org/10.1016/B978-0-08-100314-5.00017-8.

[33] Henning Almstedt, Torsten-Ulf Kern, David Segletes, Michael Loehr. The role of advanced fracture mechanics evaluation methods for turbine components. In *Proceedings of the ASME Turbo Expo 2016: Turbomachinery Technical Conference and Exposition. Volume 8: Microturbines, Turbochargers and Small Turbomachines; Steam Turbines*, Seoul, South Korea, June 2016. ASME. doi: https://doi.org/10.1115/GT2016-57339.

[34] Albert Bagaviev. Integrity assessment of high pressure steam turbine casing. *Materials at High Temperatures*, 28(3):205–211, 2011. doi: 10.3184/096034011X13123717298084.

[35] Zachary Dyer, George C. Altland. An application of metal plasticity in finite element modeling to predict the low-cycle fatigue life of a high-pressure steam turbine casing. In *Proceedings of the ASME Turbo Expo 2014: Turbine*

Technical Conference and Exposition. Volume 1B: Marine; Microturbines, Turbochargers and Small Turbomachines; Steam Turbines, Düsseldorf, Germany, June 2014. ASME. doi: https://doi.org/10.1115/GT2014-26140.

[36] Mariusz Banaszkiewicz. The low-cycle fatigue life assessment method for online monitoring of steam turbine rotors. *International Journal of Fatigue*, 113:311 – 323, 2018. ISSN 0142-1123. doi: https://doi.org/10.1016/j.ijfatigue.2018.02.032.

[37] Jan Hakl and Ondrej Bielak and Tomáš Vlasák. Residual life assessment of steam turbine casing containing crack defect. *International Journal of Pressure Vessels and Piping*, 78(11):977 – 984, 2001. ISSN 0308-0161. doi: https://doi.org/10.1016/S0308-0161(01)00112-0.

[38] S. R. Holdsworth. Creep-fatigue properties of high temperature turbine steels. *Materials at High Temperatures*, 18(4):261–265, 2001. doi: 10.1179/mht.2001.028.

[39] B. Fournier, M. Salvi, F. Dalle, Y. De Carlan, C. Caës, M. Sauzay, and A. Pineau. Lifetime prediction of 9-12%Cr martensitic steels subjected to creep-fatigue at high temperature. *International Journal of Fatigue*, 32(6):971–978, 2010. ISSN 01421123. doi: 10.1016/j.ijfatigue.2009.10.017.

[40] B. Fournier and F. Dalle and M. Sauzay and J. Longour and M. Salvi and C. Caës and I. Tourniè and P.-F. Giroux and S.-H. Kim. Comparison of various 9-12%Cr steels under fatigue and creep-fatigue loadings at high temperature. *Materials Science and Engineering: A*, 528(22):6934 – 6945, 2011. ISSN 0921-5093. doi: https://doi.org/10.1016/j.msea.2011.05.046.

[41] Krishna Guguloth, S. Sivaprasad, D. Chakrabarti, and S. Tarafder. Low-cyclic fatigue behavior of modified 9Cr-1Mo steel at elevated temperature. *Materials Science and Engineering: A*, 604:196 – 206, 2014. ISSN 0921-5093. doi: https://doi.org/10.1016/j.msea.2014.02.076.

[42] R. Mishnev, N. Dudova, and R. Kaibyshev. Low cycle fatigue behavior of a 10cr-2w-mo-3co-nbv steel. *International Journal of Fatigue*, 83:344 – 355, 2016. ISSN 0142-1123. doi: https://doi.org/10.1016/j.ijfatigue.2015.11.008.

[43] R. Mishnev, N. Dudova, and R. Kaibyshev. Effect of the strain rate on the low cycle fatigue behavior of a 10Cr-2W-Mo-3Co-NbV steel at °C. *International Journal of Fatigue*, 100:113 – 125, 2017. ISSN 0142-1123. doi: https://doi.org/10.1016/j.ijfatigue.2017.03.025.

[44] Preeti Verma, Joysurya Basu, N.C. Santhi Srinivas, and Vakil Singh. Deformation behavior of modified 9Cr-1Mo steel under low cycle fatigue at 600 °C. *Materials Characterization*, 131:244 – 252, 2017. ISSN 1044-5803. doi: https://doi.org/10.1016/j.matchar.2017.06.024.

[45] A. Nagesha, R. Kannan, G.V.S. Sastry, R. Sandhya, Vakil Singh, K. Bhanu Sankara Rao, and M.D. Mathew. Isothermal and thermomechanical fatigue studies on a modified 9cr-1mo ferritic martensitic steel. *Materials Science and Engineering: A*, 554:95 – 104, 2012. ISSN 0921-5093. doi: https://doi.org/10.1016/j.msea.2012.06.021.

[46] Richard A. Barrett, Christopher J. Hyde, Padraic E. O'Donoghue, and Sean B. Leen. Thermomechanical fatigue in 9-12cr steels: Life prediction models and the effect of tensile dwell periods. *International Journal of Fatigue*, 126:335 – 345, 2019. ISSN 0142-1123. doi: https://doi.org/10.1016/j.ijfatigue.2019.05.007.

[47] Norman E. Dowling, Stephen L. Kampe, and Milo V. Kral. *Mechanical Behavior of Materials: Engineering Methods for Deformation, Fracture, and Fatigue, Global Edition*. Pearson Education Limited, 5 edition, 2020. ISBN 978-1-292-27935-0.

[48] ISO 12106:2003(E). Metallic materials – Fatigue testing – Axial-strain-controlled method. Standard, International Organization for Standardization, Geneva, CH, march 2003.

[49] ASTM E606-92(2004)e1. Standard Practice for Strain-Controlled Fatigue Testing. Standard, ASTM International, West Conshohocken, PA, 2004.

[50] ISO 12111:2011(E). Metallic materials–Fatigue testing–Strain-controlled thermomechanical fatigue testing method. Standard, International Organization for Standardization, Geneva, CH, August 2011.

[51] S. S. Manson and G. R. Halford. *Fatigue and durability of structural materials*. ASM International, Materials Park, Ohio 44073-0002, May 2007. ISBN 978-0-87170-825-0.

[52] Ted L. Anderson. *Fracture Mechanics: Fundamentals and Applications*. CRC Press, 4 edition, 2017. ISBN 978-1-4987-2813-3.

[53] Jordi Loureiro-Homs, David Gustafsson, Per Almroth, Kjell Simonsson, Robert Eriksson, and Daniel Leidermark. Accounting for initial plastic deformation for fatigue crack growth predictions under tmf loading condition. *International Journal of Fatigue*, 136:105569, 2020. ISSN 0142-1123. doi: https://doi.org/10.1016/j.ijfatigue.2020.105569.

[54] ASTM E647-13a. Standard Test Method for Measurement of Fatigue Crack Growth Rates. Standard, ASTM International, West Conshohocken, PA, 2013.

[55] P. Paris and F. Erdogan. A Critical Analysis of Crack Propagation Laws. *Journal of Basic Engineering*, 85(4):528–533, 12 1963. ISSN 0021-9223. doi: https://doi.org/10.1115/1.3656900.

[56] P. Almroth, D. Gustafsson, J. Loureiro Homs, and K. Simonsson. Out-of-phase thermo-mechanical fatigue crack growth and the effect of the compressive minimum load level on crack closure at notches. *International Journal of Fatigue*, 141:105906, 2020. ISSN 0142-1123. doi: https://doi.org/10.1016/j.ijfatigue.2020.105906.

[57] Walter Illg and Arthur J. Mcevily. The rate of fatigue-crack propagation for two aluminum alloys under completely reversed loading. NASA Technical Note D-52, Langley Research Center, Langley Field, Va., 1959. URL `https://hdl.handle.net/2027/uiug.30112106741124`.

[58] Elber Wolf. Fatigue crack closure under cyclic tension. *Eng. Fract. Mech.*, 2 (1):37 – 45, 1970. ISSN 0013-7944. doi: https://doi.org/10.1016/0013-7944(70)90028-7.

[59] R. Pippan and A. Hohenwarter. Fatigue crack closure: a review of the physical phenomena. *Fatigue & Fracture of Engineering Materials & Structures*, 40 (4):471–495, 2017. doi: https://doi.org/10.1111/ffe.12578.

[60] Kiran Solanki, S.R. Daniewicz, and J.C. Newman. Finite element analysis of plasticity-induced fatigue crack closure: an overview. *Engineering Fracture Mechanics*, 71(2):149 – 171, 2004. ISSN 0013-7944. doi: https://doi.org/10.1016/S0013-7944(03)00099-7.

[61] Konjengbam Darunkumar Singh, Matthew Roger Parry, and Ian Sinclair. A short summary on finite element modelling of fatigue crack closure. *Journal of Mechanical Science and Technology*, 25(12):3015 – 3024, 2011. ISSN 1976-3824. doi: https://doi.org/10.1007/s12206-011-0826-9.

[62] F. Palmert, J. Moverare, and D. Gustafsson. Thermomechanical fatigue crack growth in a single crystal nickel base superalloy. *Int. J. Fatigue*, 122:184–198, 2019. doi: 10.1016/j.ijfatigue.2019.01.014.

[63] Jordi Loureiro-Homs, Per Almroth, Frans Palmert, David Gustafsson, Kjell Simonsson, Robert Eriksson, and Daniel Leidermark. Accounting for crack closure effects in tmf crack growth tests with extended hold times in gas turbine blade alloys. *International Journal of Fatigue*, 142:105917, 2021. ISSN 0142-1123. doi: https://doi.org/10.1016/j.ijfatigue.2020.105917.

[64] R.C. McClung and H. Sehitoglu. On the finite element analysis of fatigue crack closure–2. numerical results. *Engineering Fracture Mechanics*, 33(2):253 – 272, 1989. ISSN 0013-7944. doi: https://doi.org/10.1016/0013-7944(89)90028-3.

[65] S. S. Manson and G. R. Halford. *Fatigue and Durability of Metals at High Temperatures*. ASM International, Materials Park, Ohio 44073-0002, May 2009. ISBN 978-0-87170-718-5.

[66] E. Vacchieri. Review: Creep-fatigue interaction testing and damage assessment for high temperature materials. In *Reference Module in Materials Science and Materials Engineering*. Elsevier, 2016. ISBN 978-0-12-803581-8. doi: https://doi.org/10.1016/B978-0-12-803581-8.04046-7.

[67] R.P. Skelton. Creep-fatigue interactions (crack initiation). In *Reference Module in Materials Science and Materials Engineering*. Elsevier, 2016. ISBN 978-0-12-803581-8. doi: https://doi.org/10.1016/B978-0-12-803581-8.00911-5.

[68] ISO 12108:2002(E). Metallic materials – Fatigue testing – Fatigue crack growth method. Standard, International Organization for Standardization, Geneva, CH, December 2002.

[69] ASTM E1457-07. Standard Test Method for Measurement of Creep Crack Growth Times in Metals. Standard, ASTM International, West Conshohocken, PA, 2007.

[70] S. Stekovic, J.P. Jones, B. Engel, M.T. Whittaker, V. Norman, J.P. Rouse, S. Pattison, C.J. Hyde, P. HÃ¤rnman, R.J. Lancaster, D. Leidermark, and J. Moverare. Devtmf - towards code of practice for thermo-mechanical fatigue crack growth. *International Journal of Fatigue*, 138:105675, 2020. ISSN 0142-1123. doi: https://doi.org/10.1016/j.ijfatigue.2020.105675.

[71] J. Palmer, J. Jones, A. Dyer, R. Smith, R. Lancaster, and M. Whittaker. Development of test facilities for thermo-mechanical fatigue testing. *International Journal of Fatigue*, 121:208 – 218, 2019. ISSN 0142-1123. doi: https://doi.org/10.1016/j.ijfatigue.2018.12.015.

[72] S. Jacques, M. Lynch, A. Wisbey, S. Stekovic, and S. Williams. Development of fatigue crack growth testing under thermo-mechanical fatigue conditions. *Materials at High Temperatures*, 30(1):49–61, 2013. doi: https://doi.org/10.3184/096034013X13631093463744.

[73] ASTM E2368-10. Standard Practice for Strain Controlled Thermomechanical Fatigue Testing. Standard, ASTM International, West Conshohocken, PA, 2017.

[74] Frans Palmert, Per Almroth, David Gustafsson, Jordi Loureiro-Homs, Ashok Saxena, and Johan Moverare. Modelling the crack growth behaviour of a single crystal nickel base superalloy under tmf loading with long dwell times. *International Journal of Fatigue*, 144:106074, 2021. ISSN 0142-1123. doi: https://doi.org/10.1016/j.ijfatigue.2020.106074.

[75] D. Ewest, P. Almroth, B. Sjödin, D. Leidermark, and K. Simonsson. Isothermal and thermomechanical fatigue crack propagation in both virgin and thermally aged haynes 230. *International Journal of Fatigue*, 120:96 – 106, 2019. ISSN 0142-1123. doi: https://doi.org/10.1016/j.ijfatigue.2018.11.004.

[76] D. Ewest, P. Almroth, B. Sjödin, K. Simonsson, D. Leidermark, and J. Moverare. A modified compliance method for fatigue crack propagation applied on a single edge notch specimen. *International Journal of Fatigue*, 92:61 – 70, 2016. ISSN 0142-1123. doi: https://doi.org/10.1016/j.ijfatigue.2016.06.023.

[77] V. Norman, P. Skoglund, D. Leidermark, and J. Moverare. The transition from micro- to macrocrack growth in compacted graphite iron subjected to thermo-mechanical fatigue. *Engineering Fracture Mechanics*, 186:268 – 282, 2017. ISSN 0013-7944. doi: https://doi.org/10.1016/j.engfracmech.2017.10.017.

[78] V. Norman, S. Stekovic, J. Jones, M. Whittaker, and B. Grant. On the mechanistic difference between in-phase and out-of-phase thermo-mechanical fatigue crack growth. *International Journal of Fatigue*, 135:105528, 2020. ISSN 0142-1123. doi: https://doi.org/10.1016/j.ijfatigue.2020.105528.

[79] *FRANC3D 7.3.4*. Fracture Analysis Consultants, Inc, Ithaca, NY, USA, 2019. URL `http://www.fracanalysis.com/software.html`.

[80] *ABAQUS User's Manual, Version 2017*. Dassault Systemes, Johnston, RI, USA, 2017.

[81] K.S. Kim and R.H. Van Stone. Crack growth under thermo-mechanical and temperature gradient loads. *Engineering Fracture Mechanics*, 58(1):133 – 147, 1997. ISSN 0013-7944. doi: https://doi.org/10.1016/S0013-7944(97)00065-9.

[82] Christopher John Pretty, Mark Thomas Whitaker, and Steve John Williams. Thermo-Mechanical Fatigue Crack Growth of RR1000. *Materials*, 10(1), 2017. ISSN 1996-1944. doi: 10.3390/ma10010034.

[83] Lars Jacobsson, Christer Persson, and Solveig Melin. Thermo-mechanical fatigue crack propagation experiments in inconel 718. *International Journal of Fatigue*, 31(8):1318 – 1326, 2009. ISSN 0142-1123. doi: https://doi.org/10.1016/j.ijfatigue.2009.02.041.

[84] J. Dai, N. J. Marchand, and M. Hongoh. *Thermal Mechanical Fatigue Crack Growth in Titanium Alloys: Experiments and Modelling*, pages 187–209. ASTM International, West Conshohocken, PA, Jan 1996. ISBN 978-0-8031-5325-7. doi: 10.1520/STP16454S.

[85] Robert W. Smith and Gordon T. Smith. Thermal-fatigue crack-growth characteristics and mechanical strain cycling behavior of a-286 discaloy, and 16-25-6 austenitic steels. NASA Technical Note (TN) NASA-TN-D-479, Lewis Research Center, Cleveland, Ohio, 1960. URL `https://ntrs.nasa.gov/citations/19980227982`.

[86] M. Okazaki and T. Koizumi. Crack propagation of steels during low cycle thermal-mechanical and isothermal fatigue at elevated temperatures. *Metallurgical Transactions A*, 14A(8):1641–1648, 1983. ISSN 0013-7944. doi: https://doi.org/10.1007/BF02654392.

[87] R. M. Pelloux and N. Marchand. Thermal-mechanical fatigue behavior of nickel-base superalloys. NASA Contractor Report (CR) NASA-CR-175048, USAAVSCOM-TR-86-C-4, NAS 1.26:175048, Lewis Research Center, Cleveland, Ohio, 1986. URL `https://ntrs.nasa.gov/citations/19860015347`.

[88] Thomas Lindström, Daniel Ewest, Kjell Simonsson, Robert Eriksson, Jan-Erik Lundgren, and Daniel Leidermark. Constitutive model of an additively manufactured ductile nickel-based superalloy undergoing cyclic plasticity. *International Journal of Plasticity*, 132:102752, 2020. ISSN 0749-6419. doi: https://doi.org/10.1016/j.ijplas.2020.102752.

[89] Thomas Lindström, Mattias Calmunger, Robert Eriksson, and Daniel Leidermark. Fatigue behaviour of an additively manufactured ductile gas turbine superalloy. *Theoretical and Applied Fracture Mechanics*, 108:102604, 2020. ISSN 0167-8442. doi: https://doi.org/10.1016/j.tafmec.2020.102604.

[90] Christian Busse, Jordi Loureiro Homs, David Gustafsson, Frans Palmert, Björn Sjödin, Johan J. Moverare, Kjell Simonsson, Daniel Leidermark. A finite element study of the effect of crystal orientation and misalignment on the crack driving force in a single-crystal superalloy. In *Proceedings of the ASME Turbo Expo 2016: Turbomachinery Technical Conference and Exposition. Volume 7A: Structures and Dynamics*, page V07AT28A002, Seoul, South Korea, June 2016. ASME.

[91] Wen-Ping Wu, Shuang-Yu Li, and Yun-Li Li. An anisotropic elastic-plastic model for predicting the rafting behavior in ni-based single crystal superalloys. *Mechanics of Materials*, 132:9–17, 2019. ISSN 0167-6636. doi: https://doi.org/10.1016/j.mechmat.2019.02.009.

[92] William F. Hosford. *Mechanical Behavior of Materials*. Cambridge University Press, 2 edition, 2009. doi: 10.1017/CBO9780511810923.

[93] Tomáš Oplt, Marek Šebík, Filippo Berto, Luboš Náhlík, Pavel Pokorný, and Pavel Hutař. Strategy of plasticity induced crack closure numerical evaluation. *Theoretical and Applied Fracture Mechanics*, 102:59–69, 2019. ISSN 0167-8442. doi: https://doi.org/10.1016/j.tafmec.2019.04.004.

[94] R.C. McClung and H. Sehitoglu. On the finite element analysis of fatigue crack closure-1. basic modeling issues. *Engineering Fracture Mechanics*, 33(2): 237–252, 1989. ISSN 0013-7944. doi: https://doi.org/10.1016/0013-7944(89)90027-1.

[95] JC Newman. A finite-element analysis of fatigue crack closure. In JR Rice and PC Paris, editors, *Mechanics of Crack Growth*, pages 221 – 230. ASTM International, West Conshohocken, PA, 1976. ISBN 978-0-8031-4669-3. doi: https://doi.org/10.1520/STP33952S.

[96] R.G. Chermahini, K.N. Shivakumar, J.C. Newman, and A.F. Blom. Three-dimensional aspects of plasticity-induced fatigue crack closure. *Engineering Fracture Mechanics*, 34(2):393–401, 1989. ISSN 0013-7944. doi: https://doi.org/10.1016/0013-7944(89)90152-5.

[97] J.C. Newman, C.A. Bigelow, and K.N. Shivakumar. Three-dimensional elastic-plastic finite-element analyses of constraint variations in cracked bodies. *Engineering Fracture Mechanics*, 46(1):1–13, 1993. ISSN 0013-7944. doi: https://doi.org/10.1016/0013-7944(93)90299-8.

[98] D. Camas, J. Garcia-Manrique, F.V. Antunes, and A. Gonzalez-Herrera. Three-dimensional fatigue crack closure numerical modelling: Crack growth scheme. *Theoretical and Applied Fracture Mechanics*, 108:102623, 2020. ISSN 0167-8442. doi: https://doi.org/10.1016/j.tafmec.2020.102623.

[99] P.F.P. de Matos and D. Nowell. Numerical simulation of plasticity-induced fatigue crack closure with emphasis on the crack growth scheme: 2d and 3d analyses. *Engineering Fracture Mechanics*, 75(8):2087–2114, 2008. ISSN 0013-7944. doi: https://doi.org/10.1016/j.engfracmech.2007.10.017.

[100] D.S. Dugdale. Yielding of steel sheets containing slits. *Journal of the Mechanics and Physics of Solids*, 8(2):100–104, 1960. ISSN 0022-5096. doi: https://doi.org/10.1016/0022-5096(60)90013-2.

[101] JC Newman. A crack-closure model for predicting fatigue crack growth under aircraft spectrum loading. In JB Chang and CM Hudson, editors, *Methods and Models for Predicting Fatigue Crack Growth Under Random Loading*, pages 53 – 84. ASTM International, West Conshohocken, PA, 1981. ISBN 978-0-8031-4814-7. doi: https://doi.org/10.1520/STP28334S.

[102] B. Budiansky and J. W. Hutchinson. Analysis of closure in fatigue crack growth. *J. Appl. Mech.*, 45(2):267–276, 1978. doi: https://doi.org/10.1115/1.3424286.

[103] Carl Fischer, Christoph Schweizer, and Thomas Seifert. Assessment of fatigue crack closure under in-phase and out-of-phase thermomechanical fatigue loading using a temperature dependent strip yield model. *International Journal of Fatigue*, 78:22–30, 2015. ISSN 0142-1123. doi: https://doi.org/10.1016/j.ijfatigue.2015.03.022.

[104] Gabriel P. Potirniche. A closure model for predicting crack growth under creep-fatigue loading. *International Journal of Fatigue*, 125:58–71, 2019. ISSN 0142-1123. doi: https://doi.org/10.1016/j.ijfatigue.2019.03.029.

Part II

Appended Papers

Papers

The papers associated with this thesis have been removed for copyright reasons. For more details about these see:

http://urn.kb.se/resolve?urn=urn:nbn:se:liu:diva-173354

FACULTY OF SCIENCE AND ENGINEERING

Linköping Studies in Science and Technology
Licentiate Thesis No. 1900, 2021

Solid Mechanics, Department of Management and Engineering

Linköping University
SE-581 83 Linköping, Sweden

www.liu.se

LINKÖPING UNIVERSITY